Bloom Raiders: Understanding the massive phytoplankton blooms over the Australian-Antarctic Ridge

Cruise report from *Nathaniel B. Palmer* NBP2411

Kevin R. Arrigo, Chief Scientist
Stanford University

Introduction

The Southern Ocean (SO) is the largest of the three high nutrient-low chlorophyll (HNLC) regions of the global ocean where low trace metal concentrations, especially dissolved iron (dFe, <0.2 nm), limit phytoplankton growth (Martin et al. 1990, De Baar et al. 1995, Arrigo et al. 2003, Boyd et al. 2007, 2012, Alderkamp et al. 2015). Despite comprising ~26% of the global ocean area, the SO currently accounts for ~40% of total anthropogenic CO_2 uptake by the oceans (Frölicher et al. 2014, Landschützer et al. 2015). This influx of atmospheric CO_2 is facilitated by Ekman transport of cool surface waters northward and their subsequent subduction below the surface, as well as an active biological pump, whereby the CO_2 fixed by phytoplankton, the primary producers of marine food webs, eventually sinks to depth (Sweeney 2003, Takahashi et al. 2009). Understanding the impact of environmental forcing on net primary production (NPP) is critical for predicting the future uptake of atmospheric CO_2 in the SO.

NPP in the SO is patchy (Fig. 1), varying by an order of magnitude between the productive continental shelves, where DFe that is convectively mixed to the surface each winter fuels rapid phytoplankton growth (Smith & Gordon 1997, Arrigo et al. 1999), and the more oligotrophic Antarctic Circumpolar Current (ACC) region to the north (Moore & Abbott 2000, Arrigo et al. 2008a, Arrigo and Van Dijken 2015). However, even within the ACC (bounded to the north by the Sub-Antarctic Front, SAF and to the south by the Southern Boundary of the ACC, SBACC, Orsi et al. 1995) there are areas that exhibit anomalously high phytoplankton biomass and NPP compared to surrounding waters. Some of these are well understood, such as blooms in the Scotia Sea and Kerguelen Plateau where phytoplankton growth is stimulated by sediment-derived dFe mixed into surface waters as the ACC flows over shallow topography (Blain et al. 2001, 2007). The other large phytoplankton bloom (~300,000 km^2) in the ACC was recently observed in deep waters of the northwestern Ross Sea above the Australian-Antarctic Ridge (AAR) and just north of the SBACC (Schine et al. 2021) and has received comparatively little attention. We do know that this AAR bloom is a hot spot for upper trophic level activity, especially for krill and whales (Tynan et al. 1998, Andrews-Goff et al. 2018).

We sampled the AAR bloom for the first time during our Phantastic I cruise in 2014 (Schine et al. 2021) and discovered that beneath the bloom, sub-thermocline concentrations of dFe were unusually high for the region (>0.3 nM). Satellite images extending back to 1998 show that the AAR bloom is a recurring feature, forming each spring in the same location (Fig. 1), suggesting that it receives a recurring supply of dFe from some consistent but unknown source. Processes that could add dFe to SO surface waters include sediment resuspension (Blain et al. 2007), glacier/iceberg melt (Smith et al. 2007, Arrigo et al. 2015), release from melting seasonal sea-ice (Lannuzel et al. 2008), atmospheric dust deposition (Duce & Tindale 1991), volcanism (Gaiero et al. 2003), and hydrothermal activity (Klunder et al. 2011).

Schine et al. (2021) argue that because the AAR bloom forms at the same place every year and is relatively far from the Antarctic coast, its dFe source is unlikely to be glacier/iceberg melt, atmospheric dust deposition, or subaerial volcanism. The bloom is located at the northern edge of the sea ice zone where melting ice could introduce dFe into surface waters (Lannuzel et al. 2016). Alternatively, vertical advection associated with the SBACC could bring high dFe

concentrations in Upper Circumpolar Deep Water (UCDW) closer to the surface and stimulate phytoplankton growth. But why would either of these processes be restricted, year after year, to this single location? Notably, the bloom is located over the AAR and downstream of two hydrothermally active ridge segments, KR1 and KR2 (Fig. 1) suggesting a possible hydrothermal dFe source. Furthermore, the elevated dFe concentrations below the thermocline are associated with an anomalous water mass that is fresher, colder, and more oxygen-rich than waters at the same density outside of the bloom. This suggests that the source for the water mass with elevated dFe associated with the bloom is different from that of the surrounding waters. Unfortunately, tracers of hydrothermal activity (e.g., ^{3}He) were not measured during our Phantastic I cruise so we cannot be sure of its importance. Furthermore, the AAR bloom was sampled for only a short period of time and the processes responsible for bringing dFe to the surface were not investigated.
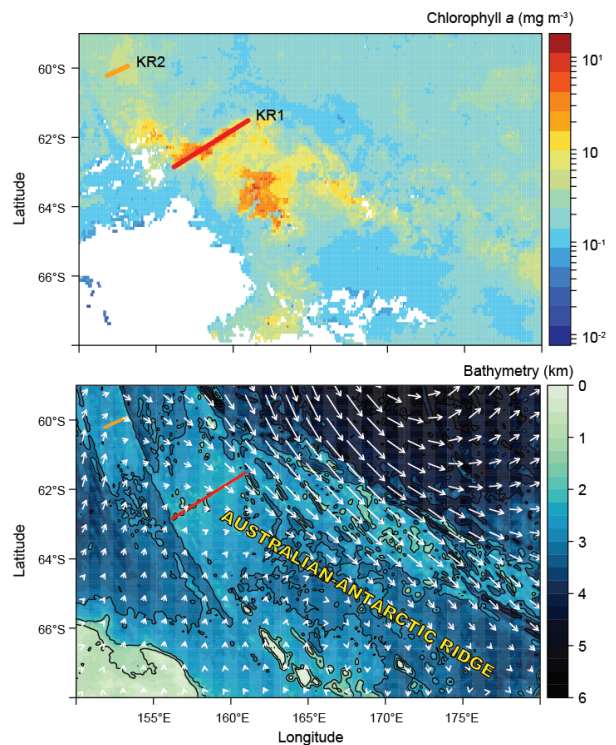

Fig. 1. Top. Location of active vent fields KR1 and KR2 along the AAR. Bottom. Flow fields over bathymetry showing that the bloom is downstream of KR1 and KR2 along the AAR.

It was previously thought that most Fe from deep-ocean hydrothermalism is inaccessible to phytoplankton because of the precipitation of Fe-rich particulates that cannot reach the surface ocean (Elderfield & Schultz 1996). However, more recent evidence suggests that dFe from hydrothermal vents is an important source of dFe (Mackey et al. 2002, Boyle et al. 2005, Statham et al. 2005, Boyle & Jenkins 2008, Bennett et al. 2008, Toner et al. 2009) to the ocean and this Fe may reach the surface and contribute substantially to biological productivity (Tagliabue et al. 2016). Tagliabue et al. (2010) estimate that deep hydrothermal input enhances surface water dFe concentrations globally by 3%, and much more locally. For the AAR bloom, upwelling of deep water associated with AAR topography could provide a mechanism for vertical transport of deep hydrothermal dFe to the surface (Sokolov & Rintoul 2007). Furthermore, the position of the bloom adjacent to the SBACC and its associated steeply sloping isopycnals (Orsi et al. 1995) favors the upward transport of hydrothermal Fe.

Hydrothermal Fe is especially important in the SO, contributing 20×10^9 g of `new' dFe annually to the ocean inventory, equivalent to 37-79% of non-sediment inputs (Tagliabue et al. 2010, Tagliabue and Resing 2016). Overall, these model-based results suggest that the addition of hydrothermal Fe can dramatically increase SO NPP, with extra dFe fueling 20-30% more export (3-5 g C m^{-2} yr^{-1}) (Tagliabue et al. 2010). Some of the first observational evidence of the importance of this process in the SO was reported by Ardyna et al. (2019), who used Argo float data and modeling to indicate that hydrothermally produced Fe along the Southwest Indian Ridge upwells into surface waters via flow-topography interactions and stimulates massive phytoplankton blooms, enhancing the regional food supply for the pelagic ecosystem and stimulating the biological pump (Ardyna et al. 2019).

2

Based on these recent observations, the goal of our study was to investigate the factors controlling the development of the large AAR phytoplankton bloom that forms regularly in the northwestern Ross Sea. The annual reoccurrence of the AAR bloom in this location presents a rare opportunity to intensively study the suite of physical and chemical processes that greatly enhance surface NPP at the confluence of the sea ice edge, a major oceanographic front, and an active hydrothermal vent site. Specifically, we endeavored to study the fate of hydrothermal plumes along the segment of the AAR where the AAR bloom forms, determine the relative importance of different sources supplying dFe to surface waters, and quantify the impact of the AAR bloom on biological pump processes such as NPP.

Overview of Study

The cruise took place from 13 December 2024 to 3 February 2025, beginning and ending in Lyttleton, NZ. Sampling by the research team (Table 1) was focused on a grid centered along the AAR and extending from 60.5-62.5°S latitude and 155-165°E longitude, the mean location of the phytoplankton bloom each year. The sampling grid consisted of six approximately parallel transects with 7-10 stations along each (Fig. 2). We sampled the full grid twice, and then we intensively sampled three areas of particular interest within the grid (details below).

Table 1. Science team for the Bloom Raiders cruise

Biology

Kevin Arrigo	Stanford University	P. I., Chief Scientist
Gert van Dijken	Stanford University	
James Lauer	Stanford University	
Ali Palm	Stanford University	
Sicada Sloan	Stanford University	
Cara Askren	Stanford University	
Jenny Jackson	Stanford University	
Riley Moulton	UCSC	

Physics

Leif Thomas	Stanford University	P. I., not onboard
Amanda Vanegas Ledesma	Stanford University	
Lemona Niu	Stanford University	

Chemistry

Joe Resing	UW	P. I., not onboard
Randelle Bundy	UW	P. I., not onboard
Tamara Baumberger	NOAA	P. I.
Nathan Buck	UW	
Pam Barrett	UW	
Patrick Monreal	UW	
Jess Davis	UW	
Sophie Jenness	UW	
Stevie Walker	UW	

Outreach

Bhavna Rawal	Polar STEAM Educator Fellow	
Madeline Blount	Polar STEAM Artist	

At the 146 hydrographic survey stations within our study region, we measured vertical profiles of temperature, salinity, currents, light, and chlorophyll *a* (Chl *a*) concentration, particle backscattering (using a light scattering sensor, LSS), and oxidation-reduction potential (ORP sensor). We also collected seawater samples at six depths to measure phytoplankton abundance/species/size (PlanktoScope), algal physiology using the fast repetition rate fluorometer (FRRf), NPP, and particulate organic carbon and nitrogen (POC/PON). At about half of the stations, we collected water at 12 depths to measure trace metals, helium, and methane concentrations from the trace metal clean (TMC) rosette.

During transits, we continuously measured atmospheric conditions as well as sea surface temperature, salinity, nitrate, oxygen, pCO$_2$, and Chl *a* fluorescence from the various ship's systems to provide detailed maps of these parameters.
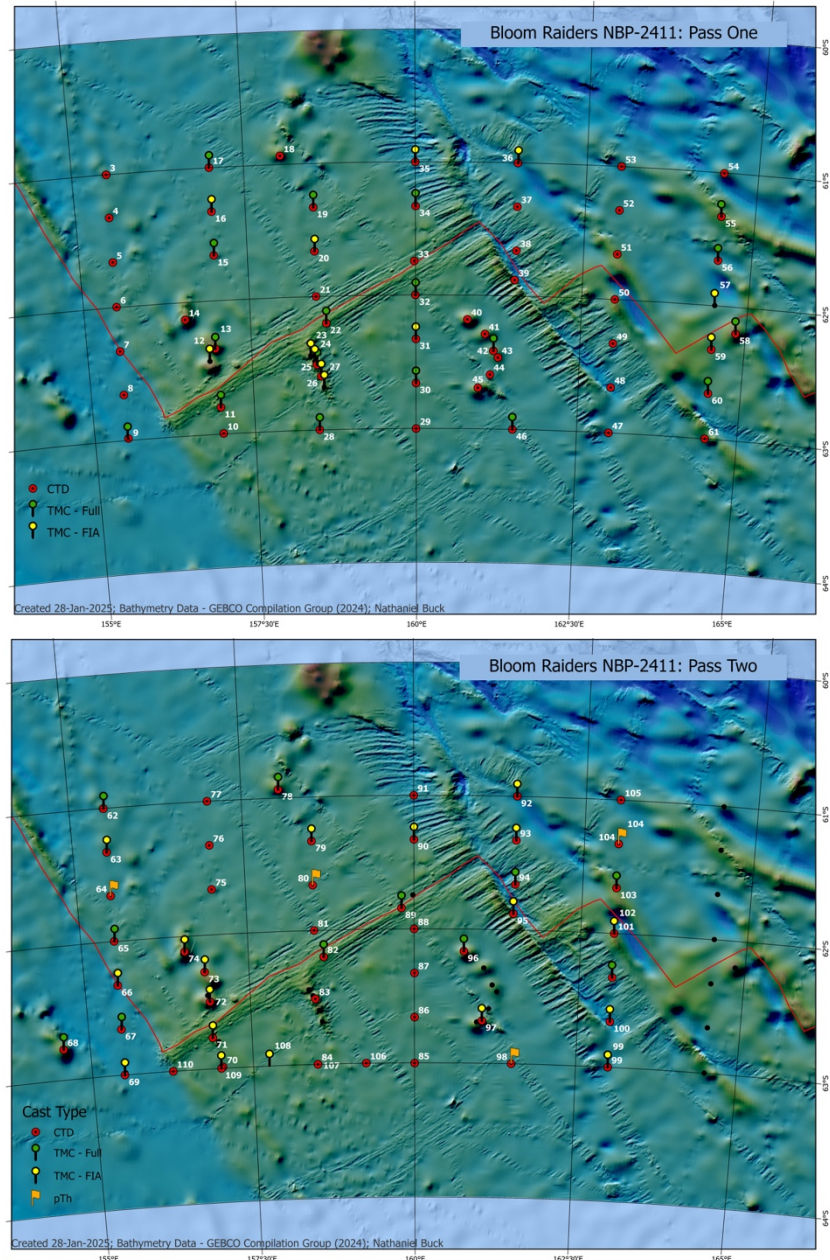

Fig. 2. Top. Location of stations during the first occupation of the grid. Bottom. Location of stations during the second occupation of the grid. Colors indicate bathymetry (red = shallower, blue = deeper).

Week 1

We arrived at our first north-south transect in our study area along 155°E on December 19. At the first station along the transect (St. 3), we deployed the conventional CTD, trace metal-clean pump, and released an Argo float. All performed well and we were able to collect samples for trace metal concentrations in surface waters, as well as vertical profiles of Chl *a*, POC/PON, inorganic nutrients, FRRF, and phytoplankton community composition from the conventional CTD. At the southernmost station (St. 9), we obtained our first TMC cast profile and deployed the conventional CTD to a depth of 200 m.

On December 21, we steamed 78 km to the east to begin our second north-south transect along 157°E. St. 10 marked the start of the transect, where the conventional CTD was deployed to 2000 m. At St. 11, we again deployed both the conventional CTD (to 200 m) and the trace metal-clean CTD rosette (to 10 m above the bottom), targeting the location of a known seamount which could be a potential source of hydrothermal activity.

Week 2

The second week of the cruise started by sampling a series of seamounts clustered along the second transect (St. 12-14). We used the multi-beam system to produce high resolution maps of bottom topography and began to conduct CTD operations with the TMC and conventional CTDs near the seamounts. We obtained full water column profiles of helium and dFe, as well as inorganic nutrients and phytoplankton biomass in the upper 100 m. After sampling the seamounts, we continued north to complete the rest of the second transect, measuring similar quantities along the way.

On the third transect, we headed south again to sample a series of volcanoes that intersected our transect. The conventional CTDs were deployed at every station and the TMC rosette at approximately every other station. We sampled a few more stations along the transect and used the multibeam to more accurately map the seafloor around the undersea volcanoes.

We then continued to the fourth transect, where we were able to complete the first four stations (four conventional and two TMC CTDs) before heading south to the ice edge to get out of the way of an oncoming storm. Along the way, we did a detailed multibeam survey of a series of seamounts located between the fourth and fifth transect.

Week 3

In the early morning of December 30, we headed back north to complete the fourth transect that was interrupted by the storm. We began science operations at St. 33, where we continued our pattern of conducting conventional CTDs at every station and the TMC rosette at approximately every other station. We completed the rest of transect four and headed east to begin sampling transect five.

Preliminary data analyses from the LSS and ORP sensors during earlier transects showed evidence of hydrothermal plumes of dFe associated with the seamounts along transect two. Our first bioassay experiments showed clear evidence of dFe limitation of phytoplankton growth on transect two after four days of incubation. This was consistent with measurements made with the FRRF that consistently showed the phytoplankton were dFe-stressed in surface waters.

Due to high seas, we were unable to conduct TMC rosette sampling along much of the fifth (St. 36-46) and sixth (St. 47-53) transects (we only sampled at one location). Instead, we sampled using the conventional CTD and used the LSS and ORP sensors to detect evidence of hydrothermal activity. This information was used to direct sampling when we sampled the region again later in the cruise. Water samples were still used to characterize phytoplankton and nutrient distributions along this transect, despite our lack of dFe data.

Near the end of the week, the weather cleared long enough for us to get a full complement of conventional and trace metal CTDs along the seventh transect (St. 54-61). We were also able to deploy an Argo float and two surface drifters along this transect.

To avoid another storm, and because we were approaching the midpoint of the cruise, we ended the grid at St. 61 and head back to the northwest to begin sampling the entire grid again.

Week 4

By January 6, we had reached the start of the sampling grid along transect one. Science operations began at the northern end of the first transect. This time, we were able to deploy the

conventional CTD and the TMC CTD rosette at every station along the transect, with preliminary dFe profiles showing low concentrations (<0.2 nm) over most of the water column. The same was true for Chl *a* concentrations along that transect.

Sea ice was still present at the southern end of the first and second transects and so phytoplankton concentrations remained low. Heading north along the second transect, we sampled above a seamount (St. 72) that extended upwards to within 700 m of the surface. The ORP and LSS sensors showed evidence of hydrothermal activity at this site and we measured dFe concentrations of >8 nM in waters as shallow as 450 m. This site was very close to the KR1 ridge which had been identified in the past as the site of significant hydrothermal activity. We were able to complete the second transect after having deployed the conventional CTD and the TMC CTD rosette at every station.

Bioassay experiments continued to show clear evidence of dFe limitation of phytoplankton growth along all our transects, consistent with measurements made with the FRRF that consistently showed that the phytoplankton in surface waters were dFe stressed.

After completing transect two, we headed east to start sampling the third transect. We sampled stations heading south and weather remained relatively calm for the entire transect. Again, we were able to deploy the conventional CTD and the TMC CTD rosette at every station.

At Sta. 82 along the third transect, we saw the most dramatic evidence thus far of a large hydrothermal plume. This plume was much more intense and much thicker than the plume we sampled at St. 72, extending from 600-1100 m below the surface. We used water from this and two subsequent shallower casts to begin some bioassay experiments, testing the hypothesis that dFe in the hydrothermal plume is sufficient to stimulate phytoplankton growth.

Week 5

We completed the third transect on January 12 and proceeded east to the fourth transect. We continued to conduct conventional CTDs at every station and the TMC rosette at approximately every other station, focusing on those stations that were missed during the first occupation of the transect. We observed elevated dFe concentrations at several locations along the transect, both near the bottom and further up in the water column. These high-dFe stations were generally located near the KR1 ridge and seemed to be associated with nearby seamounts and underwater volcanos.

We completed the fourth transect and continued on to the fifth. We had not been able to deploy the TMC rosette at about half of the stations during the first grid occupation of that transect, so we focused our TMC sampling on those stations during this pass. We measured elevated dFe at a few of the stations, and once again, these stations were associated with either a ridge or a seamount. We also observed the highest phytoplankton concentrations to date (although not that high) along this transect, near the sites with elevated dFe.

Multiple bioassay experiments continued to show clear evidence of dFe limitation of phytoplankton growth along all our transects. A bioassay to assess manganese co-limitation with dFe suggested that manganese was not a co-limiting factor for phytoplankton growth. These bioassay results were consistent with measurements made with the FRRF that consistently showed that the phytoplankton in surface waters were dFe stressed.

In order to give ourselves sufficient time to go back and resample some of the regions of interest we observed previously, we decided to drop the last line of the grid. After completing the grid for the second time, we headed east to begin resampling an east-west transect along the southern boundary of our study region to determine the flow rate of the Balleny Gyre into our study region. We wanted to know if dFe from the shelf was advecting into our study region from the south.

Week 6

On January 20, we began resampling an east-west transect along the southern boundary of our study region. Weather prevented us from performing any TMC casts, but we were able to obtain a good hydrographic section using the conventional CTD. We were also able to deploy two drifters along this transect, which will be used to gauge the trajectory of the flow over time.

After completing the southern transect, we headed to the northwest to resample the seamount near the southern portion of the second transect and very close to the KR1 ridge. We had measured dFe concentrations of 10 nM within the caldera of the seamount but we wanted to know if this high dFe signal was being transported further afield. We created a "control volume" by sampling in a square pattern around the seamount using both the conventional CTD and the ADCP. We will use these data to calculate the volume flux into and out of this control volume. We measured vertical profiles of dFe within the caldera, along the rim of the caldera and along its flank. Amazingly, dF concentrations were >200 nM near the floor of the caldera and as high as 8 nM at a depth of 400 m below the ocean surface.

At around midnight on January 24, we were able to begin sampling in the region where we previously observed (St. 82) a large plume of dFe in the water column to trace its origin. Along the way, we conducted a couple of stations along the KR1 ridge. At a station 10 km southwest of location of St. 82, we observed the largest LSS signal up to that point on the cruise. The layer of particle-laden water was more than 1300 m thick and extended to within 300 m of the ocean surface. We continued sampling in a high resolution (10-15 km) grid pattern around the station with the high LSS signal to pinpoint the source of the hydrothermal fluid. This was done with both TMC and conventional CTDs. We observed high LSS values at a number of stations (St. 131 had elevated LSS over a depth of 1700 m) and were able to determine that the plume originated just south of the KR1 line and moved toward the northeast across the ridge. DFe concentrations were extremely high, with waters having >10 nM of dFe ascending from the bottom to within 200 m of the surface.

In summary, we were successful in identifying the source of dFe that has been fueling phytoplankton blooms in the AAR region, likely for decades. Our data clearly point to a hydrothermal origin and a physical mechanism (probably eddy generation-see below) for bringing the dFe from almost 2 km deep into near surface waters. We were also able to show that the phytoplankton were dFe-stressed over much of the study region, except for the region near the hydrothermal plume. For some reason, the phytoplankton bloom had still not developed anywhere within our study grid by the time of the cruise, perhaps because of the frequent storms and deep mixed layers we encountered almost everywhere. This could have reduced average light levels in surface waters and slowed phytoplankton growth. Further analysis of our physiological and environmental data will be required to address this issue.

Below are some details and highlights from the various subcomponents of the research effort associated with the Bloom Raiders cruise.

Satellite Data
P. I.: Arrigo
At Sea: Van Dijken

During the cruise, a variety of satellite remote sensing products were used. An automated system was set up at Stanford University to have the remote sensing data emailed to the research vessel. It is also available on the project website (http://ocean.stanford.edu/aar_bloom/). Chl *a* images were used to show the spatial distribution of phytoplankton and to track the development of the phytoplankton bloom. Sea level height anomalies were used to visualize and track eddies,

fronts, and other mesoscale features. Sea ice concentration and sea surface temperature images were also used to characterize our study area.

Chl *a* data were acquired from NASA's Ocean Color website (https://oceancolor.gsfc.nasa.gov/). The near-real-time daily level 3 binned data product was used. A daily merged composite was generated from the following ocean color sensors (if available at run time): Aqua on the MODIS satellite, three VIIRS sensors (on JPSS1, JPSS2 and SNPP satellites) and two OLCI sensors (on Sentinel S3A and S3B). Due to persistent cloud cover which resulted in limited data coverage, a rolling 8-day image was generated as well, which was calculated daily as the mean of the eight most recent daily images. Final Chl *a* images were combined with sea ice concentration obtained from the NOAA/NSIDC data repository (Near-Real-Time NOAA/NSIDC Climate Data Record of Passive Microwave Sea Ice Concentration - National Snow and Ice Data Center, https://nsidc.org/data/g10016/versions/2). Sea surface temperature was downloaded from PODAAC-JPL; the product used was GHRSST (Group for High Resolution Sea Surface Temperature) Level 4 MUR Global Foundation SST Analysis (v4.1, https://podaac.jpl.nasa.gov/dataset/MUR-JPL-L4-GLOB-v4.1). Sea level height anomaly was downloaded from Copernicus; the product used was Near-Real-Time Global Ocean Gridded L 4 Sea Surface Heights And Derived Variables (https://data.marine.copernicus.eu/product/SEALEVEL_GLO_PHY_L4_NRT_008_046/description).

Fig. 3. Combined Chl *a* and sea ice image of our study region for the time period 2-9 January 2025.

All images were mapped to two common projections, one showing a zoomed in view of our study area and one showing a wider view. All images are available in png, tiff, netCDF and Google Earth (kml) format. Fig. 3 is an example of a combined Chl *a* and sea ice concentration image obtained before, during, and after the Bloom Raiders cruise.

Physical Oceanography
P.I.: Thomas
At Sea: Vanegas Ledesma, Niu

Objectives. The goal of this study was to characterize the origin of the dFe-rich waters that feed the AAR bloom. We aimed to collect a dataset that would allow us to identify dFe sources and characterize transport pathways towards the surface bloom. Additionally, we aimed to study possible upwelling mechanisms of dFe rich waters and retention time of surface, high-Chl *a*
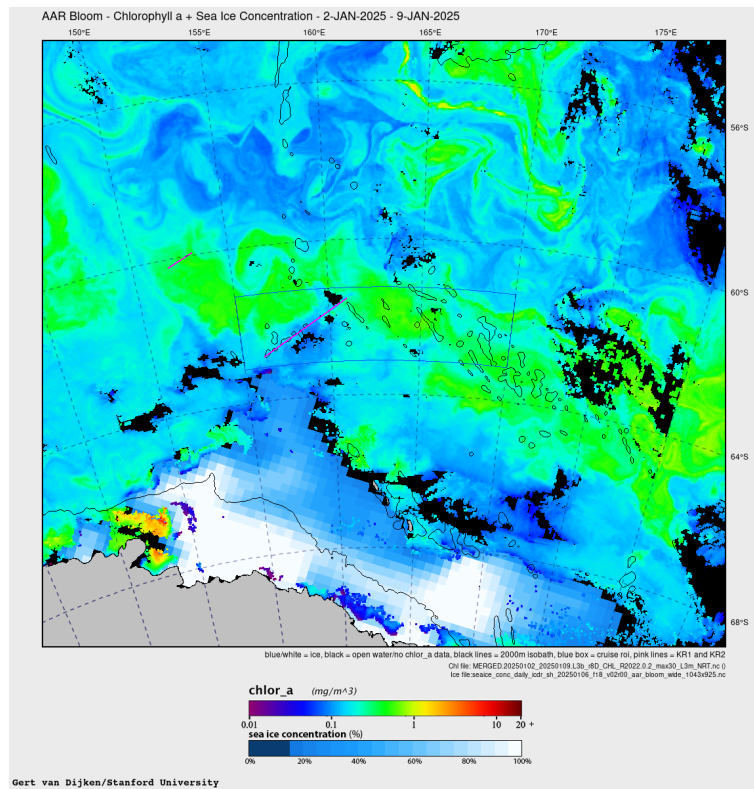
waters. We identified active hydrothermal dFe sources and transport pathways that follow local gyre circulation.

Methods
Depth Profile Casts and Water Sampling
    CTD Operation. A total of 132 CTD and 105 TMC casts were carried out over 146 stations. Upon completion of each cast, an automated script processed the raw data into a 1dp pressure-binned downcast file, an upcast file, and a full cast file. Prior to the downcast and once the CTD is submerged at 10 m under sea surface, we performed soaking for at least 200 seconds until sensors were equilibrated and stopped oscillating. At the beginning of the cruise, conductivity and temperature sensors were taking an anomalously long period to stabilize, likely due to their sensitivity to surface temperature and the salinity gradient at the soaking depth. There were a few casts where the CTD was sent down before sensors were fully equilibrated, therefore we advise that caution should be taken when interpreting the surface 10 m on these downcasts. To avoid mixing generated by the rosette itself impacting the sensor measurements, we principally relied on data generated during the downcast.

    At each of the stations on our grid, when conditions and time allowed, we conducted a CTD cast down to 200 m to sample for surface biology, followed by a TMC cast down to 2000 m to sample for helium and trace metals, including dFe. For the biology cast, we targeted six depths: 2, 10, 25, 50, 75, and 100 m. Adjustments to these depths were decided on a case-by-case basis with a goal of avoiding large density gradients and capturing the subsurface chlorophyll maximum (SCM). Each day around midday local time, we took water samples for measurements of simulated in situ primary production (SIS) and dissolved inorganic carbon (DIC).

Table 2. Sensors on the CTD casts and the configuration file names when troubleshooting for the uncalibrated conductivity sensors.

Station	Conductivity Sensor 1	Conductivity Sensor 2	Config File
123	CTD Primary	TMC Primary	NBP_2411_CTDvsTMC.xmlcon
124	CTD Primary	TMC Secondary	NBP_2411_CTDvsTMC2.xmlcon
130	CTD Secondary	TMC Primary	NBP_2411_CTDvsTMC3.xmlcon
125	CTD Secondary	TMC Secondary	NBP_2411_CTDvsTMC4.xmlcon
135-146	CTD Primary	TMC Primary	

    The two TMC conductivity sensors output salinity values very close to each other and are 0.002 PSU away from the secondary CTD conductivity sensor. However, the primary CTD sensor produced salinity values 0.008 PSU higher than the two TMC sensors (Fig. 4). Based on the swapping test we performed onboard, we believe that the CTD primary conductivity sensor needs to be recalibrated after the cruise. Before calibration is completed, all analyses should be based on the secondary conductivity sensor on the CTD or either of the sensors on the TMC.

    The CTD secondary conductivity sensor broke after the station 134 cast was recovered. The breaking occurred sometime after the CTD rosette was onboard, so all data on the station 134 CTD cast was reliable. We replaced the CTD secondary conductivity sensor with the primary conductivity sensor on the TMC, thereby all stations CTD cast after station 134 had the CTD primary sensor and the TMC primary sensor as the secondary conductivity sensor.

CTD Sensors and Equipment

The conventional CTD Rosette system contains twenty-four 10 L Niskin bottles and a sensor package that measures temperature, pressure, conductivity, fluorescence, oxygen, turbidity, photosynthetically available radiation (PAR), and altimetry.
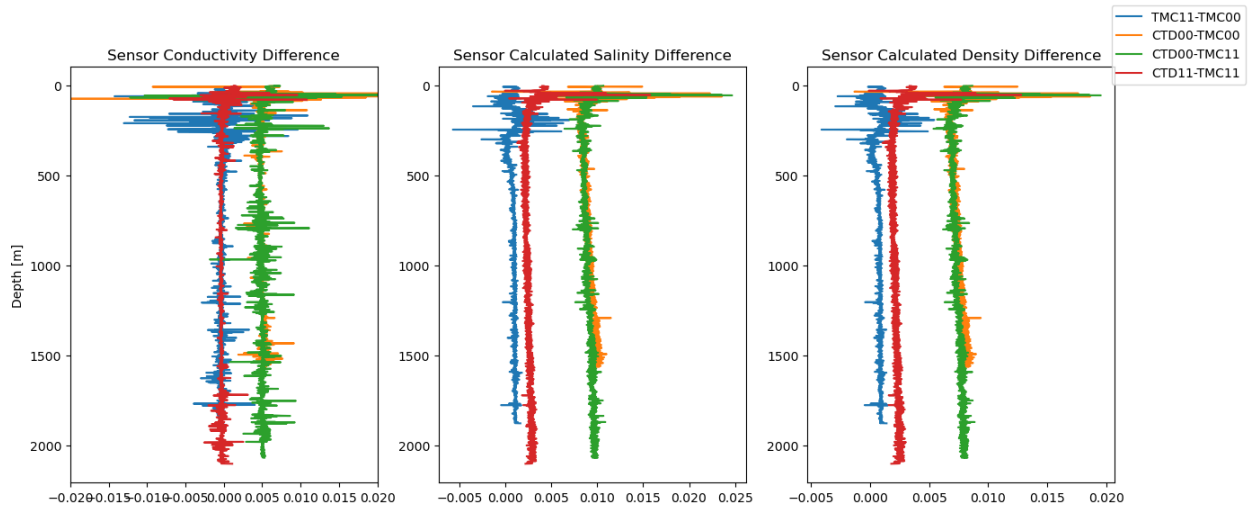

Fig. 4. Sensor comparison plots.

Table 3. Conventional CTD Sensors.

Instrument/Sensors	Model	Serial Number
CTD	Sea-Bird SBE SBE9plus	1190
Pressure	Paroscientific 410K-105	43528
Carousel Water Sampler	Sea-Bird SBE32	1097
Primary Temperature (T1)	Sea-Bird SBE SBE3	5025
Secondary Temperature (T2)	Sea-Bird SBE SBE3	5034
Primary Pump	Sea-Bird SBE5T	55109
Secondary Pump	Sea-Bird SBE5T	51646
Primary Conductivity (C1)	Sea-Bird SBE SBE4	3534
Secondary Conductivity (C2)	Sea-Bird SBE SBE4	2065
Altimeter	Valeport VA500	51519
PAR Sensor	General Oceanics QCP2350	70492
Primary Dissolved Oxygen	Sea-Bird SBE SBE43	0139
Secondary Dissolved Oxygen	Sea-Bird SBE SBE43	0196
Transmisometter	WetLabs C-STAR	CST-1316DR
Fluorometer	WetLabs	FLRTD-397
SPAR Sensor	Biospherical QSR-2200	20531
Deck Unit	Sea-Bird SBE11plus	0288

Trace Metal Conductivity, Temperature, Depth recorder (TMCTD) Operation

The TMC CTD rosette system contains twelve 10 L Niskin bottles as well as a sensor package similar to the conventional CTD.

Table 4. TMC CTD Sensors.

Instrument/Sensors	Model	Serial Number	Dates
TMC	Sea-Bird SBE SBE9plus	1315	
Pressure	Paroscientific 410k-134	138503	
Carousel Water Sampler	Sea-Bird SBE32	32-1052	
Carousel Water Sampler	Sea-Bird SBE32	32-1177	From 01/04/2025 to 01/12/2025
Primary Temperature (T1)	Sea-Bird SBE SBE3	5851	
Secondary Temperature (T2)	Sea-Bird SBE SBE1	5977	
Primary Pump	Sea-Bird SBE5T	8275	
Secondary Pump	Sea-Bird SBE5T	9000	
Primary Conductivity (C1)	Sea-Bird SBE SBE4	4666	
Secondary Conductivity (C2)	Sea-Bird SBE SBE4	4670	
Altimeter	Valeport VA500	56636	
PAR Sensor	General Oceanics QCP2350	70558	
Primary Dissolved Oxygen	Sea-Bird SBE SBE43	2267	
Secondary Dissolved Oxygen	Sea-Bird SBE SBE43	3178	
Transmisometter	WetLabs C-STAR	CST-557DR	
Fluorometer	WetLabs	FLRTD-397	
SPAR Sensor	Biospherical QSR-2200	20531	
Deck Unit	Sea-Bird SBE11plus	0768	

Acoustic Doppler Current Profiler (ADCP)
Equipment and Techniques

The shipboard ADCP system (University of Hawaii Data Acquisition System, UHDAS) infers instantaneous water velocity from the Doppler frequency shift of an acoustic ping. The system consists of a 75 kHz Ocean Surveyor and 150 kHz Narrow Band operating alternately in narrow bandwidth and broad bandwidth modes. Onboard data processing uses a set of codes and system configurations, the Common Ocean Data Access System (CODAS), to process the dataset based on the specified ping type. Data are processed and binned into 5 minute increments in near real-time.
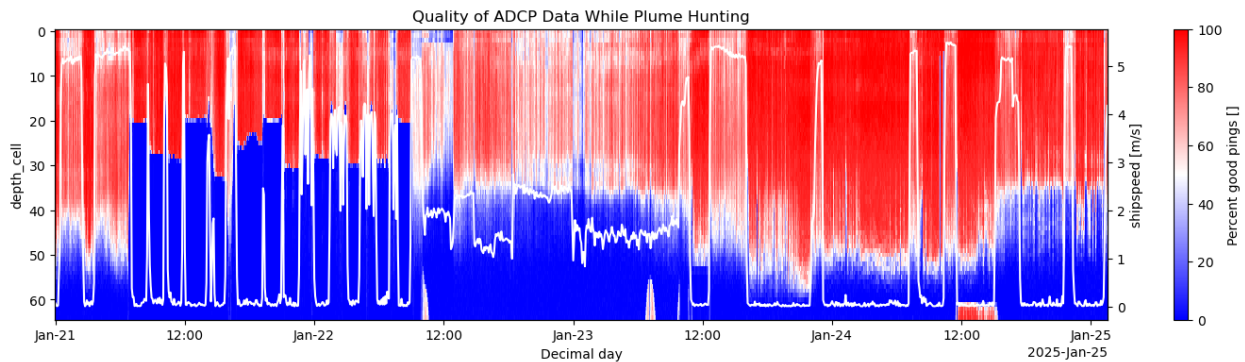

Fig. 5. ADCP Data quality time series. 50-100% good ping values are the recommended range.

Data Processing and Future Analysis

Due to storms and rough seas and the presence of sea ice in the high latitudes, the ADCP data quality sometimes was reduced to <50% of good pings, which is the recommended threshold for data quality assessment, particularly when the ship operates at full speed of around 10 knots (Fig. 5). Post-cruise processing will be needed for data of lower quality.

ADCP data collected around the shallow seamounts will be used to observe near inertial waves generated from flow-bathymetry interactions. We also performed surveys around an Fe-rich crater four times to capture the flow in and out of the crater with a goal of estimating dFe flux. ADCP velocity data will allow us to quantify mixing associated with the plume signals, explaining pathways for dFe to reach the surface from the ~2000 m deep ridge.

Multibeam E122 echo sounder Mapping
Equipment and Techniques

The EM 122 system is designed to perform high resolution acoustical seabed mapping as well as water column backscatter. The EM 122 operates at sonar frequencies of around 12 kHz with a ping rate of up to 5 Hz and an angular coverage of about 150°. The 4° receiver of each ping returns 144 beams, giving 216 soundings in high density mode, while the 1° or 2° receivers give 288/576 beams in dual swath mode, providing 432/864 soundings in high density mode. In typical ocean depths, this system achieves a sounding spacing of about 50 m across and along with swath width in the order of 30,000 m, by using FM chirps.

The Knudsen chirp sub bottom profiler onboard also measures the water column depth. It is often differs by10-100 m from the multibeam echo sounder. We collected both for reference of water column depths.

Surveying and Data Processing

In addition to multibeam data collected along our cruise tracks, we completed detailed multibeam surveys of a crater, a ridge/vent field, as well as some shallow seamounts of research interest. We performed preliminary de-pinging on the boat for these bathymetries of special interest. Intermittent storm conditions and sea ice significantly interfered with the multibeam echo sounder beams. Therefore, deep cleaning of the multibeam data is needed post-cruise.

Sampling strategies:

Radiator grid: To capture the mesoscale distribution of Chl *a*, dFe, and other biogeochemical tracers, we performed two passes of a radiator grid. The grid encompassed an area of roughly 500 km x 230 km and the stations were about 40 km apart. By doing the radiator grid twice, we were able to capture some of the temporal variability of the bloom: we observed different physical and biological dynamics in each pass. During these two passes, we observed interesting small-scale features that were revisited during the last 10 days of the cruise. These included: a signature of the cyclonic circulation of the Balleny Gyre and its role in nutrient transport, an active, shallow (600 m) caldera where high dFe values were observed near the bottom, and a plume of high LSS signature and high dFe content observed along the ridge.

Balleny Gyre Transect: The large-scale circulation of the area is given by the cyclonic circulation of the Balleny Gyre. This gyre is a western branch of the Ross Gyre, and its circulation is mostly modulated by the ACC interacting with local bathymetry. To capture the incoming flux from the gyre to the bloom region, we performed a longitudinal transect consisting of five CTD stations (St. 106 to 110). We measured a full dFe profile at one of these stations. This transect is located on the southern and western side of the grid; its position was chosen to be collocated with the western branch of the Balleny Gyre, as estimated by physical measurements performed during the first two passes of the radiator grid. We estimated the position of the gyre

by studying the depth of isopycnal surfaces, as it is well known that the cyclonic circulation of the gyre bends the isopycnals towards the surface.

Caldera Flux Study: We used the multibeam data to map the bathymetry of an underwater caldera where concentrations of dFe were >200 nM near the bottom. We then performed a small-scale survey of the caldera over a 24 h period where we aimed to produce a dataset that can be used to calculate the flux of dFe from the caldera to the surrounding waters. We did three full casts inside the caldera where we measured dfe and other chemical tracers. These casts show that dFe, temperature, and salinity are well mixed inside the crater. It is possible that the caldera waters get transported outside with the aid of internal waves and tides. To capture this variability, we did two casts on the rim of the caldera. We choose the area where the bathymetry of the rim was shallowest, which constitutes the depth at which caldera waters first get mixed with the outside. The casts inside the caldera were performed about 7 h apart. Hence, comparing the physical and chemical properties of the two casts should allow us to identify the effect of tidal variability on transport of tracers from the caldera to the outside. To characterize flow bathymetry interactions, we did two passes across the caldera with the ship to obtain ADCP data in the zonal and meridional direction. We also did four boxes surrounding the caldera with the ship to obtain velocity data from the ADCP. All the boxes were completed within a 12 h period, which will allow us to identify the semidiurnal variability of the flow and calculate the tidal and inertial motion of the currents surrounding the caldera. This should allow us to build a box model where we can use ADCP velocities, CTD sensor data, and measured geochemical tracers to obtain the dFe flux of from the caldera to the surrounding waters. We also deployed two drifters on top of the caldera which will allow us to calculate dispersion of the surface waters and further constrain our model.

Plume Study: During the second pass of the radiator grid, we observed a signal of high particle anomaly (LSS) that correlated with high concentrations of dFe in St. 82. We revisited this station and surveyed the plume area between Sts. 124 and 146. We mapped the extent of the bloom using the LSS and ORP sensors and used CTD sensors to capture the water mass properties of the high LSS and dFe waters and sampled for dFe and gasses at these stations.

Preliminary Observations
Density fronts and Chlorophyll Observations
On the west side of the radiator grid, we were closer to the ice edge, which resulted in more stratified surface waters which limited the biological productivity on the southern side of the radiator track (Fig. 6, left). On the east side of the track, storms had more time to mix surface
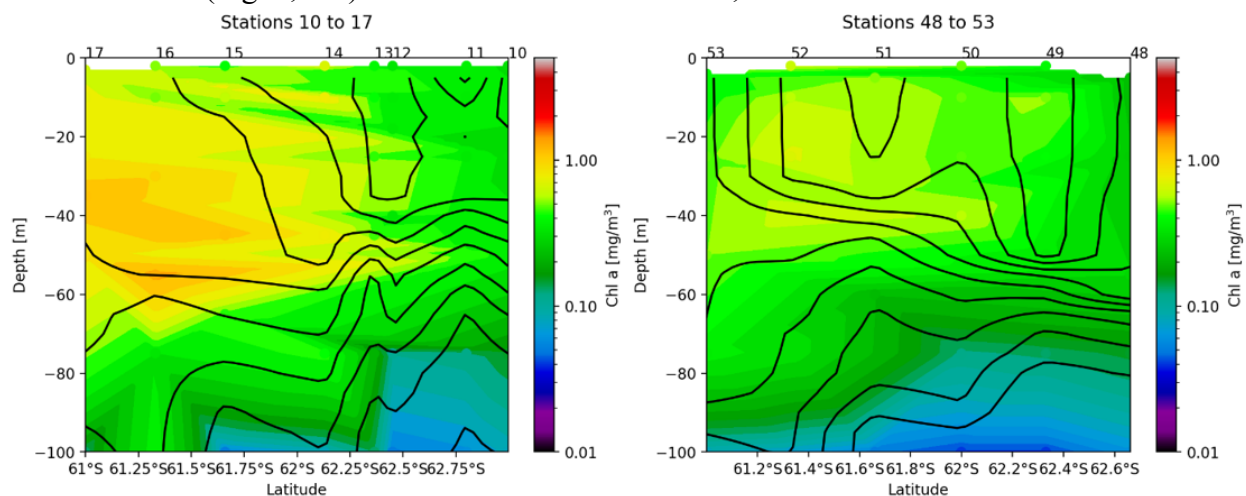

Fig. 6. Chlorophyll *a* along lines 2 and 6 of the radiator track with density contours in black.
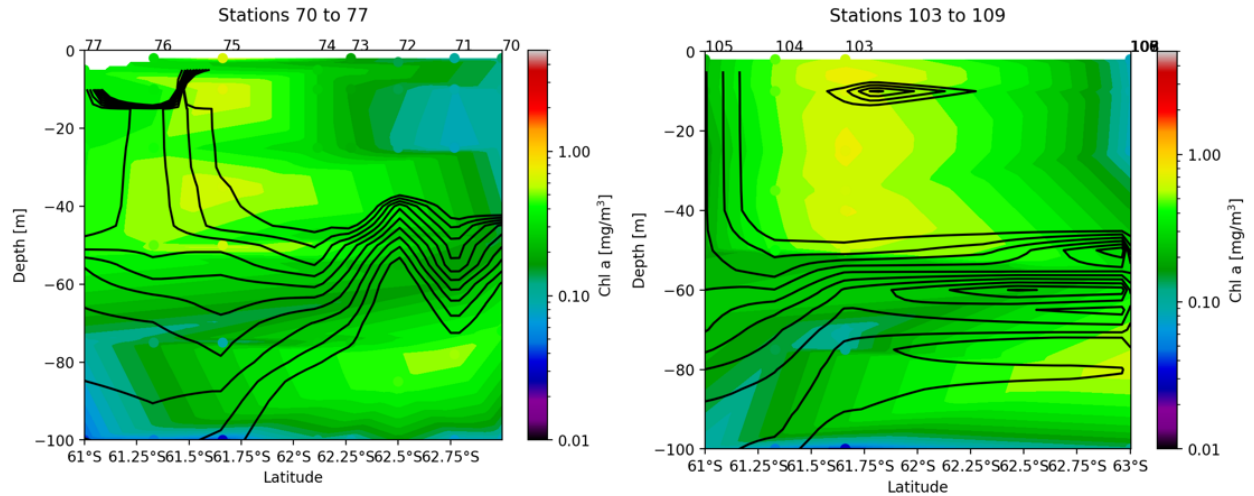
13

Fig. 7. Chlorophyll *a* along lines 10 and 14 of the radiator track with density contours in black. These lines are the same as lines 2 and 6 shown in Fig.1, but as measured during the second pass.

waters, which resulted in surface fronts that allowed nutrients to upwell to the surface and increase production in the south of the domain (Fig. 6, right). On both the southeast and southwest sides of the domain, at about 60 m depth, strongly stratified waters were likely preventing nutrients from reaching the surface and therefore halting primary production.

A comparison between transects 2 and 6, sampled during the first pass, with transects 10 and 14, sampled during the second pass, allowed us to observe the time evolution of the bloom. On both transects 10 and 14 it can be noted the development of a SCM on the southern side of the domain, below the layer of strong stratification at 60 m (Fig. 7). On the northern side of the domain the surface fronts have moved more towards the north, allowing for a more uniform layer of high Chl *a*.

Water Mass Properties of Iron-enriched Waters

Fe-enriched (but not high dFe) waters were generally observed between the 27.75 kg/m^3 and 27.82 kg/m^3 potential density surfaces and were correlated with colder and fresher waters (Fig. 8). These water mass properties are like those of Modified Circumpolar Deep Water, which is consistent with previous observations in the area.
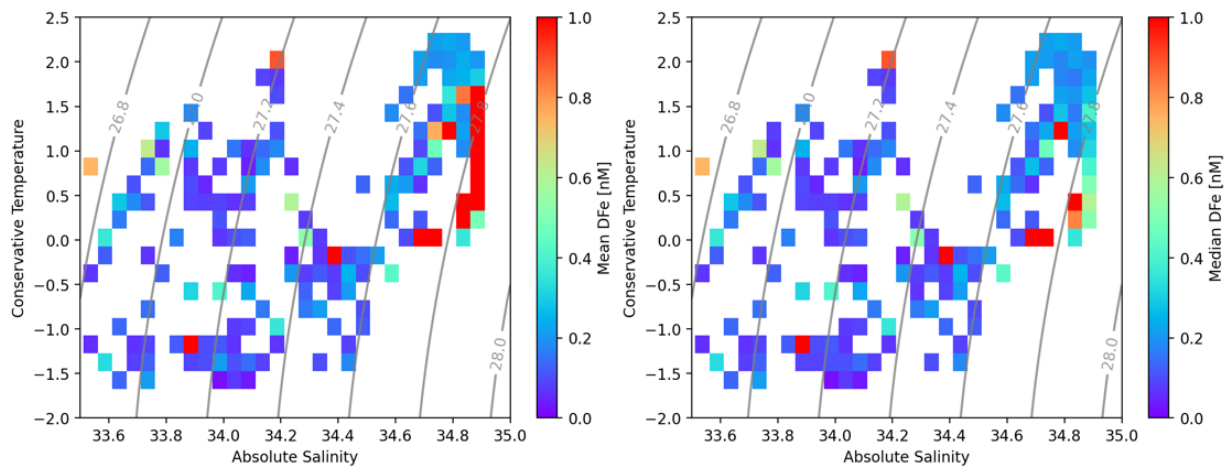

Fig. 8. T-S properties of sampled waters colored with mean and median iron concentrations.

14

Balleny Gyre Transport of Iron-enriched Waters

The doming of isopycnals reveals the structure of the Balleny Gyre (Fig. 9, left). The shallowest depth on the south side of the domain shows the center of the gyre, and waters circulate in a cyclonic direction along isopycnal depth contours. It can also be seen how Fe-enriched waters seem to be transported along this isopycnal (Fig. 9, right).
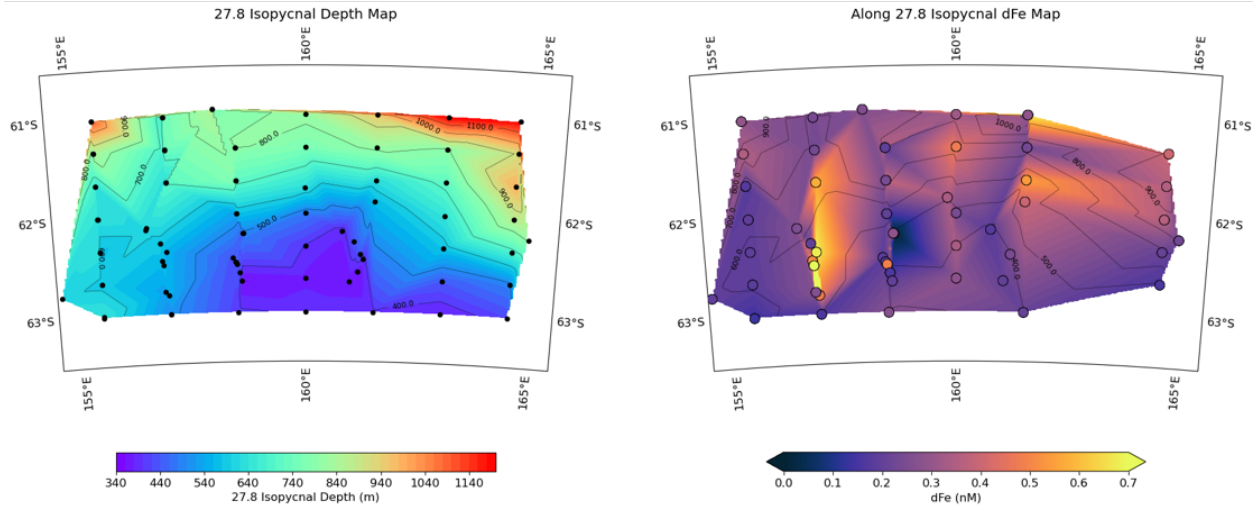

Fig. 9. Depth (left) and iron (right) on the 27.8 kg/m^3 potential density isopycnal. Black contours are isopycnal depth.

Observations of Near Inertial Waves

There is a strong near inertial forcing in the region, as revealed by the loops traced by surface drifters (Fig. 10, left). This resonance with the near inertial frequency has the potential to generate near inertial waves (NIW) forced by the wind and bottom boundary layer dynamics. There is some evidence for NIW in the ADCP data, as observed by shear bands that propagate downwards in time (Fig. 10, right), which indicates downward energy propagation.
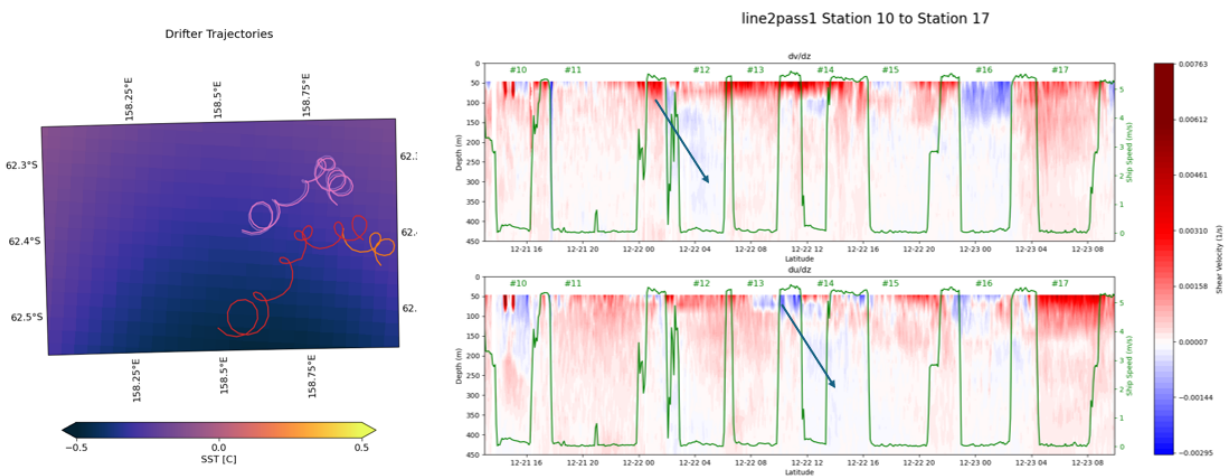

Fig. 10. Drifters trajectories (left) and vertical shear from ADCP velocities (right).

Balleny Gyre Transect Observations

The longitudinal transect taken along the western branch of the Balleny gyre shows a zonal density gradient (Fig. 11). By thermal wind balance these observations suggest the presence of a northward jet flowing from the south into our sampling grid. These fronts are collocated with elevated dFe concentrations on the east of the transect, suggesting that dFe-enriched waters are being transport by the gyre.
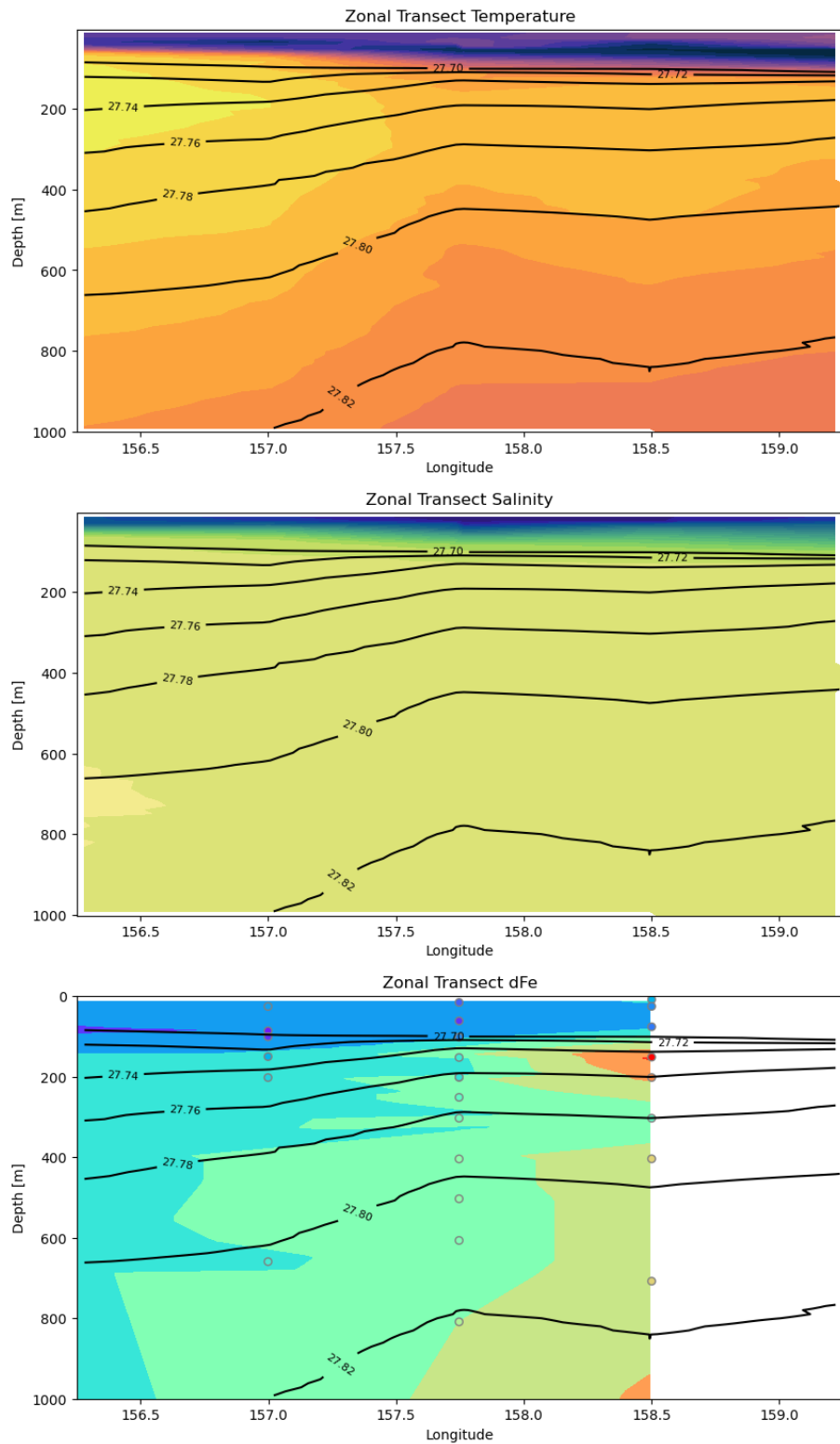

Fig. 11. Observations along the longitudinal transect on the western branch of the Balleny Gyre. Potential density (top), salinity (middle), and iron (bottom) with density contours in black.

16

Seamount Iron Observations

During the second pass of the grid, we found a shallow (500-700 m depth) caldera at station 72. We revisited the area and found high dFe concentrations both inside the caldera and on the rim (Figs. 12 and 13, right). Furthermore, waters inside the crater were generally warmer than those outside and had uniform potential temperature profiles (Fig. 12, left), which suggests that waters inside the crater are well mixed. At the rim stations, waters are more stratified in temperature (Fig. 13, left). We sampled twice on the rim of the crater, with a 7 h gap between the sampling. During the first sampling, waters were warmer and had higher dFe content than during the second sampling (Fig. 13, compare Rim 1 and Rim 2). This suggests a tidal modulation on the export of waters from inside to outside of the caldera.
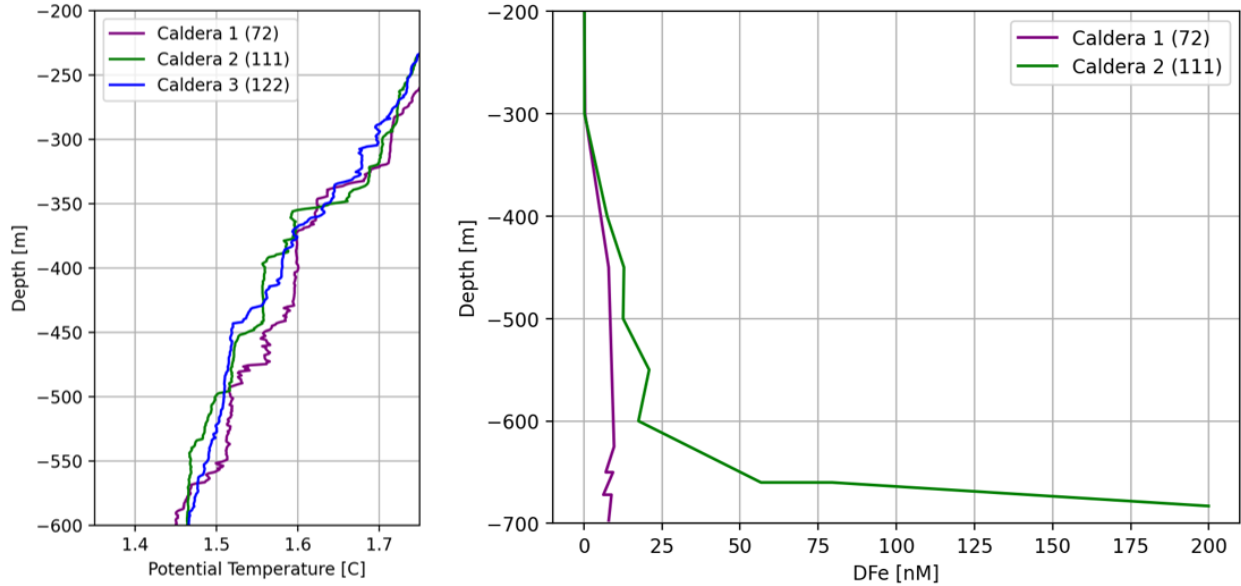

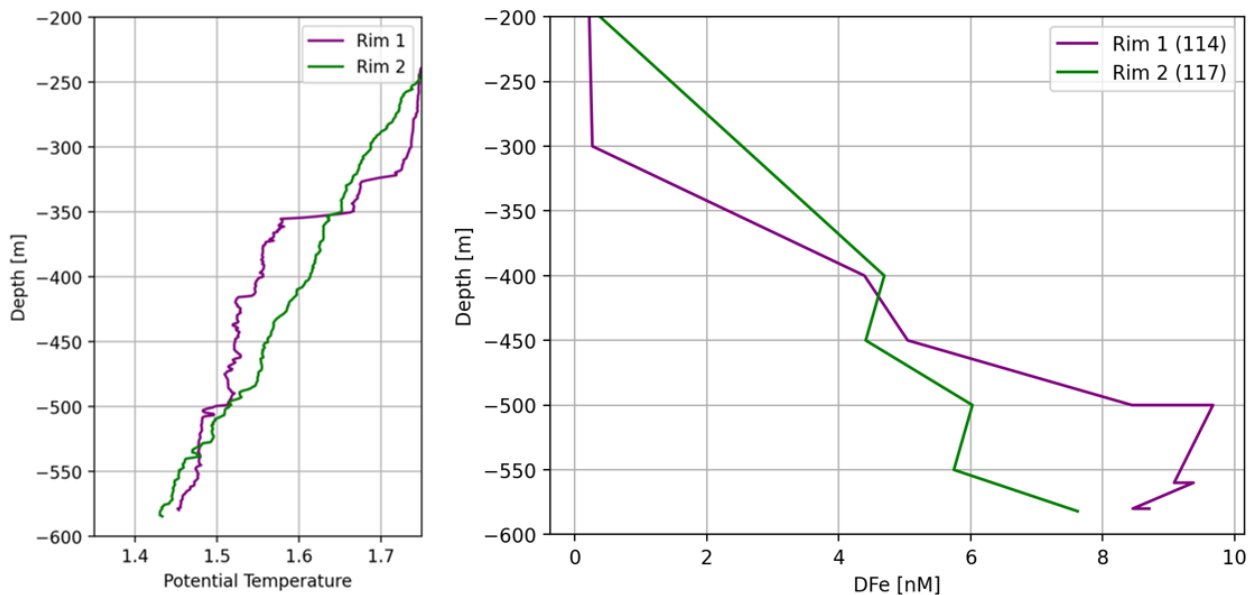Fig. 12. Potential temperature (left) and dissolved iron (right) inside the caldera.

Fig. 13. Potential temperature (left) and dissolved iron (right) outside the caldera, on its rim.

17

High LSS Iron Plume

We found a plume of high LSS signal during the second pass, in station 82. We later came back and surveyed the area. We found consistent high LSS signals and high dFe concentration on the plume waters (Fig. 14). Based on these observations we hypothesized that this is a plume of hydrothermal dFe that has spread through the water column and has been transported on the north-east direction.
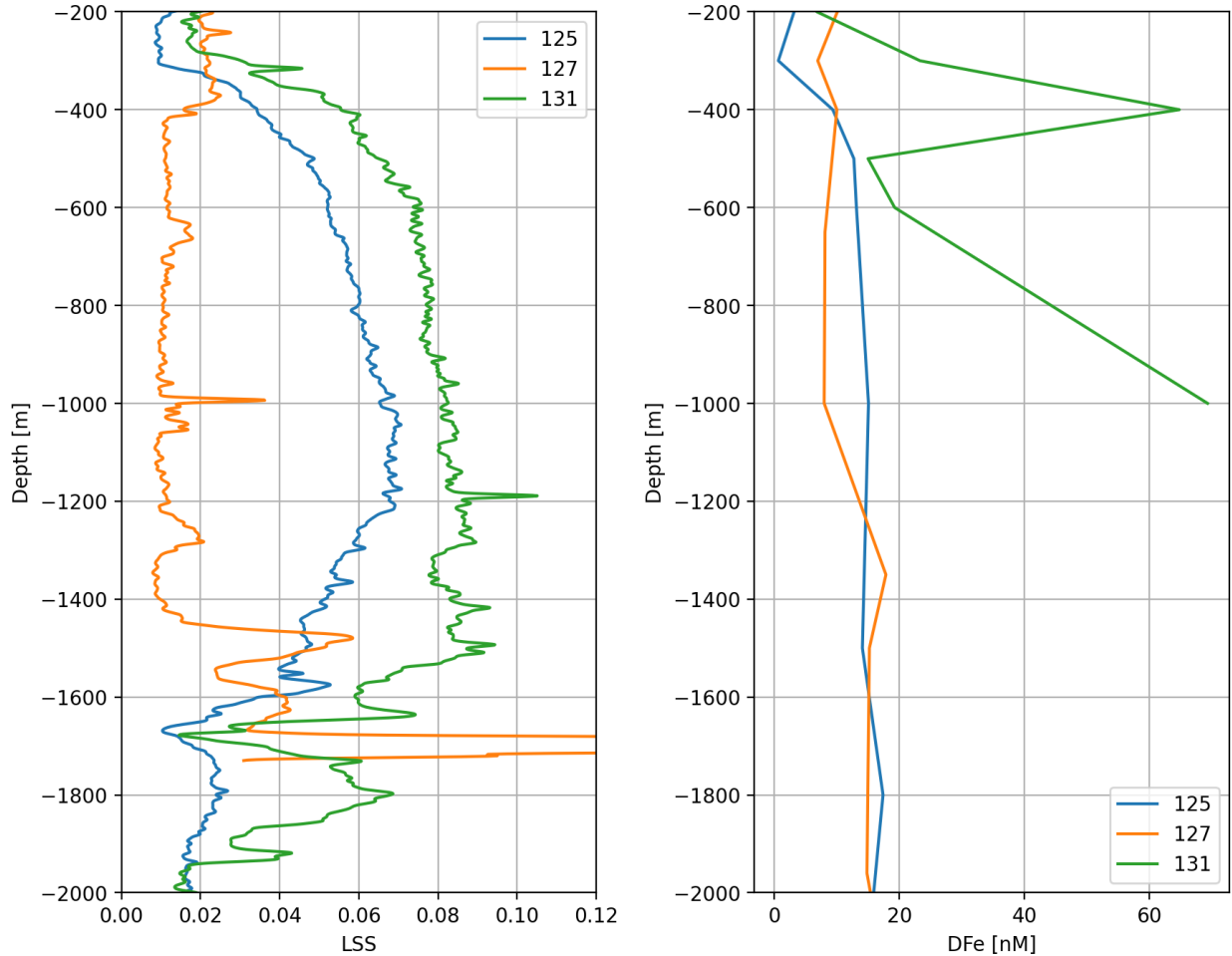

Fig. 14. LSS (left) and Dissolved Iron (right) on the plume stations

Internal Eddy Observation

Potential density contours along the ridge reveal an upward and downward bending of isopycnals centered at about 700 m depth (Fig. 15, right). This is the depth where high LSS signals and dFe concentrations were observed. The upward and downward bending of isopycnals is characteristic of internal eddies, which could form in the region due to current-topography interactions. At St. 131, high dFe was observed throughout the eddy depth, with higher concentrations on the edges of the eddy (Fig. 15, left). The internal eddy is also revealed by the depth of the isopycnals in the region. The 27.8 kg/m^3 isopycnal is bent downwards whereas the 27.82 kg/m^3 isopycnal is bent upwards (Fig. 16). These observations also suggest the presence of an internal eddy in the region with a dFe-enriched core.
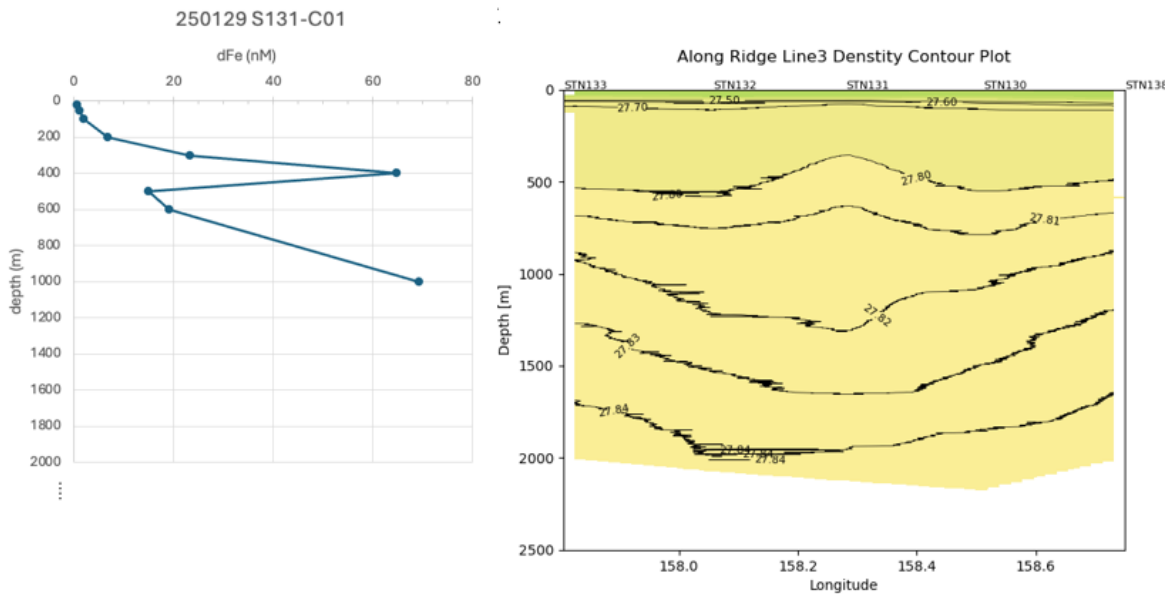
Fig. 15. Iron profile on St. 131 (left) and density contours from stations along the ridge, centered at St. 131.
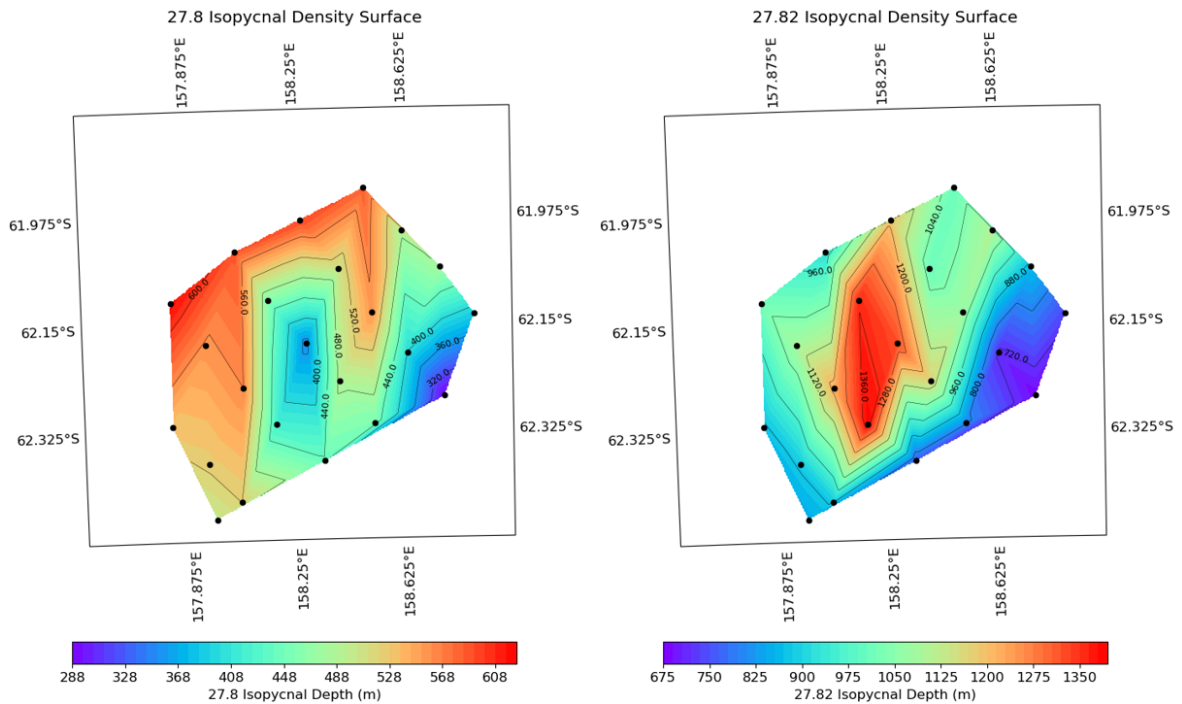

Fig. 16. Depth of 27.8 kg/m^3 (left) and 27.82 kg/m^3 (right) potential density surfaces near the high dFe plume.

Planned Research

Caldera Flux Study. We plan to use the in-situ biogeochemical measurements and data from the CTD sensor, ADCP, and drifters to calculate the dFe flux in and out the caldera observed in transect 2 and surveyed at stations 111-123. We plan to use the difference in salinity and temperature profiles of the repeated stations on the rim to estimate the tidal cycle. We suspect that tides and other bottom boundary layer dynamics are responsible for the exchange of waters

19

in and out of the caldera. Furthermore, we can use the ADCP data that we obtained by repeating the box surrounding the caldera (4 times) to obtain estimates of the mean flow and use these velocities to create a flux estimate from the caldera towards the outside. We can also use density gradients obtained from CTD data to estimate currents as given by thermal wind balance and drifter velocities to constrain the surface velocities.

Plume Hunting Study. We observed a high LSS and dFe plume between Sts. 124 and 146. We plan to study the origin of these dFe-rich waters and potentially track them back to a hydrothermal source. Additionally, we aim to characterize the mechanisms of upwelling and mixing through the water column for these dFe-rich waters. For these purposes, we will use the bathymetry data obtained by the multibeam to construct an idealized model of the circulation in the region. The model will inform us about the flow-bathymetry interactions and potential upwelling and transport mechanisms. Moreover, we intend to study the temporal and spatial scales of the plume, i.e., is this the result of an episodic volcanic eruption in the region or is there a constant source that could provide a sustainable dFe input to the bloom?

Drifter Analysis. We plan to use data from pairs of drifters we deployed to characterize dispersion of surface waters (see section on drifters below). The drifters deployed on top of seamounts will inform us about the retention time of waters on these areas. Furthermore, the drifters deployed in the Balleny Gyre will allow us to constrain the water and nutrient transport by the gyre in and out the AAR bloom.

Nutrients
P. I.: Arrigo
At Sea: Van Dijken, Arrigo

Nutrients were collected directly from the Niskin bottles in 60 mL HDPE bottles at each sampling depth within the upper 100 m. The bottles were acid washed and rinsed twice with MilliQ before use. To avoid contamination, nutrients were sampled before any other samples were taken from the Niskin bottles. The sample bottle was rinsed three times before final sample collection from the Niskin bottle. Samples were also collected from the various experiments carried out during the cruise. After collection, the bottles were put into a -20 freezer. Care was taken that they were standing upright, to prevent brine from leaking through the cap during freezing. Also, the bottles were filled just below the neck to leave enough space for expansion during freezing. Samples will be transported back to Stanford University for analysis of NO_3^-, NO_2^-, PO_4^{3-}, NH_4^+, and $Si(OH)_4$ concentrations.

Phytoplankton Biomass
P. I.: Arrigo
At Sea: Arrigo

For analysis of Chl *a*, triplicate 200 ml seawater samples were filtered onto 25 mm Whatman glass fiber filters (GF/F, 0.7 μm nominal pore size) and extracted in the dark in 5 mL of 90% acetone for 24 hrs at 3°C prior to measurement (Holm-Hansen et al. 1965) on a Turner Designs 10-AU fluorometer calibrated with pure Chl *a* (Sigma-Aldrich).

Particulate organic carbon and nitrogen (POC and PON) samples were filtered through precombusted 25 mm GF/Fs. Blank filters were made daily by passing ~25 mL of filtered (0.2 μm) seawater through GF/Fs and processing them the same as for the particulate samples. All filters were immediately dried at 60°C and stored dry until processing. Prior to analysis, samples were fumed with concentrated HCl, dried in a low-temperature oven at 60°C, and packed into tin capsules (Costech Analytical Technologies, Inc.) for analysis. Samples will be analyzed on an

Elementar vario EL cube or MICRO cube elemental analyzer (Elementar Analysensysteme GmbH, Hanau, Germany) which will be interfaced to a PDZ Europa 20-20 isotope ratio mass spectrometer (Sercon Ltd., Cheshire, UK). Calibration standards will be glutamic acid and peach leaves.

Over the course of the cruise, we obtained approximately 650 Chl a and POC/PON samples at 110 hydrographic stations. Chl a concentrations were measured onboard ship and vertical profiles at each station were obtained. Most profiles fell into one of two categories, those with a well-defined SCM and those with constant values in the mixed layer (Fig. 17).

Chl a concentrations remained low throughout the cruise, very rarely exceeding 1 µg/l at any depth and at any location. It became clear that the phytoplankton had not bloomed during the time of the cruise. Satellite imagery collected before the cruise suggest that the phytoplankton bloom had not developed prior to our arrival either. It is possible that it may begin after we depart once the surface ocean stratifies and mixed layers shallow.

Fig. 17. Top. Vertical Chl a profile exhibiting constant mixed layer values. Bottom. Vertical Chl a profile exhibiting a distinct SCM at 80 m.

Simulated in-situ Primary Production
P. I.: Arrigo
At Sea: Van Dijken

Each day, net primary production in the water column was measured using 24 h incubations in on-deck incubators, using stable isotopes of carbon and nitrogen as tracers. Samples were incubated in 1 L clear polycarbonate bottles that were spiked with 0.23 mmol $H^{13}CO_3$ and 3.0 µmol $^{15}NO_3^-$, reflecting a 10% addition relative to ambient concentrations. The bottles were covered with varying layers of neutral density screening to simulate optical depths in the water column (50%, 25%, 12.5%, 6.3%, 3.1% and 0.1% of incident light). Water from the first two optical depths were collected from the shallowest Niskin bottle (~2 m), the third and fourth optical depths from 10 m and the last two depths were collected from 25 m and the deep chlorophyll maximum, respectively. After 24 h, samples were filtered over GF/F filters that were pre-combusted in a muffle furnace for 4 h at 450C. Isotopic particulate organic carbon and nitrogen concentrations will be measured at home on a mass spectrometer. Net uptake of CO_2 and NO_3^- by phytoplankton will be calculated from isotope ratios.

Phytoplankton Physiology
P. I.: Arrigo
At Sea: Askren, Moulton

To assess algal photophysiological state, we collected samples from two depths (2 and ~25 m or SCM) and assayed for differences in photosynthesis versus irradiance characteristics using a LabSTAF FRRf, which provided estimates of maximum photosystem II (PSII) photochemical efficiency (Fv:Fm), effective cross-sectional area of PSII (σ), electron turnover time (τ) of PSII, and non-photochemical quenching (NPQ).
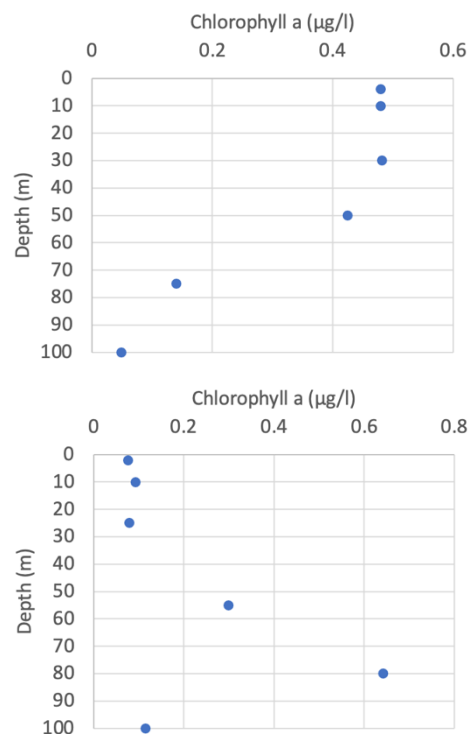
All 297 conventional CTD samples were run in Auto FLC mode. This allowed us to obtain light curves, as well as the photophysiological parameters Fo, Fm, Fv, Fv/Fm, ρ, σ, τ_{EK}, and τ_{T}, that we later compiled into a large dataset. An additional 13 samples for experiments were run in Auto FLC mode, while the remaining experimental samples (42) were run in Multi-sample mode using the manual RunSTAF setup. Each Multi-sample file contains information on between one and 15 samples, as different experiments had different numbers of samples to run at one time.

For samples run in Auto FLC mode, we collected Niskin bottle water in opaque 50 ml falcon tubes. For experimental samples, the water came from incubated bottles associated with each project. We allowed the samples to sit for at least 20 minutes on ice in the dark after collection to dark-adapt the phytoplankton prior to running the samples in the LabSTAF. We then poured some of the water from the darkened tube into a 20 ml glass cuvette to run in the sample.

Most settings in Auto FLC mode were kept as default values, but we did experiment with the step number, the high E value, turning auto high E on and off, and lowering the "up" value. We set the step number to 8-10 steps for most samples, as we found that having more steps caused the instrument to not run all steps, especially with a high E value that was set too high. Generally, we ran the deeper water samples on a high E value of between 150 and 450 µmol photons m^{-2} s^{-1}, and the shallower water samples on a high E value of between 450 and 1000 µmol photons m^{-2} s^{-1}. The variation depended on biomass in the area and often, if we found that not all steps got run on a sample with a certain high E value, we would run the sample a second time with a lower high E value to get a better light curve.

For experimental samples run in Multi-sample mode, we followed the same protocol in terms of gathering the samples in darkened tubes and dark-adapting them for 20 minutes. But for this mode, we did not need to set the step number or high E value, as we were only interested in the Fv/Fm value. This was obtained by simply putting each sample in the cuvette sequentially (washing with DI water in between) and allowing the LabSTAF to measure the value.

Preliminary results show that the average Fv/Fm across all stations was relatively low (0.23). Our highest Fv/Fm was at station 144, where the value was 0.49. Sts. 28, 9, 83, 24, 130, and 144 also had relatively high Fv/Fm values, ranging from 0.41 to 0.46. These were the only stations on our grid that experienced Fv/Fm values in the 0.4-0.5 range, but we saw many more with a value ranging from 0.30 to 0.39. Our lowest Fv/Fm value was observed at St. 56, where Fv/Fm was only 0.09. Many stations, however, exhibited values in the 0.1-0.2 range, and it was not until the end of the cruise when we measured higher concentrations of dFe in the surface waters were higher Fv/Fm values, like that seen in station 144, observed.

Phytoplankton Community Composition
P. I.: Arrigo
At Sea: Palm

We used the PlanktoScope (Pollino et al. 2022), a new low-cost flow-imaging microscope, to quantify the microplankton community composition of various discrete-volume samples collected during this cruise. The PlanktoScope consists of a peristaltic pump connected downstream of a rectangular capillary flow cell, the contents of which are imaged by a Raspberry Pi (https://www.raspberrypi.com/) with a Raspberry Pi camera in a simple optical train consisting of a tube lens and an objective lens. The peristaltic pump operates in a stop-flow imaging sequence, in which a constant-volume unit of sample is pumped through the flow cell from a sample input tube, an image is saved of the contents of the flow cell, and then another unit of sample is pumped through the flow cell, another image is saved, and so on. The acquired images of the flow cell are saved for subsequent processing to isolate cell images of individual

objects, mostly consisting of phytoplankton, which can in turn be processed to calculate morphological and taxonomic metrics about the source sample.

On our cruise, the PlanktoScope was used to analyze the 15-200 µm fraction of discrete-volume samples from Niskin bottles collected in CTD casts and from bioassay incubation experiments.

We analyzed 226 seawater samples from 146 CTD stations (typically with samples collected from the surface and from the SCM) and 155 samples from incubation experiments. Our standard protocol for processing CTD samples was to concentrate each 2000 ml sample by a factor of approximately 40-200 using a submerged 15 um filter, resulting in a concentrated suspended sample with a volume of approximately 10-50 ml depending on the visually-apparent biomass density in the sample; then to pass the >15 µm fraction of suspended sample through a 200 µm filter to remove cells too large for the PlanktoScope flow cell. If after concentration the cells were too crowded in the flow cell for imaging, filtered seawater was added for dilution. The concentration and dilution factors for each sample were recorded to enable quantitative comparison of absolute plankton counts across samples. The final samples were loaded into the PlanktoScope, which was configured to perform 400 stop-flow steps for each sample with a pumped volume of 0.02 mL per stop-flow step, resulting in 0.83 mL of sample imaged across a total of 400 raw images from 8 mL of each sample. After image acquisition, images are segmented into individual cell object images. Typically, the raw image datasets acquired from low-biomass samples contained approx. 100 - 2000 individual objects in the >15 µm fraction (estimated from the PlanktoScope software segmentation algorithm to isolate individual objects from raw images), while datasets from high-biomass samples usually contained approx. 2000-25000 individual objects in the >15 µm fraction.

These images will be uploaded into EcoTaxa, a web application for plankton image classification that uses trained models and human verification, to identify the cells. These data will then be used to classify differences and changes in phytoplankton community composition across study sites and throughout bioassay incubation experiments. (Irisson et al. 2022).

Trace Metal Chemistry
P. I.: Bundy, Resing, Baumberger
At Sea: Buck, Barnett, Monreal, Davis, Walker, Jenness

CTD operations. CTD operations were conducted using the ship's conventional rosette with 24 Ocean Test Equipment (OTE) Standard water sampling bottles as well as the ship's trace metal clean (TMC) rosette with 12 General Oceanics GO-FLO bottles (provided by P. I. Resing) or 12 OTE water sampler bottles (provided by P. I. Bundy). In total, 106 TMC casts and 134 conventional CTD casts were conducted. Both CTD rosette packages were equipped with sensors to measure temperature, salinity, fluorescence (WET labs ECO-AFL/FL), and oxygen (SBE-43). To ensure data collection on hydrothermal anomalies in the water column, each CTD was also equipped with one PMEL-supplied high sensitivity optical backscatter sensor (OBS; Seapoint Turbidity Meters 0-5 NTU range) and one PMEL oxidation-reduction potential (ORP) sensor (all supplied by Sharon Walker, NOAA PMEL). The ORP sensor mounted on the conventional rosette (ORP-09) started to malfunction from St. 15 onwards. Attempts to clean the sensor did not improve its performance. Whenever a conventional CTD but no TMC cast was planned for a given station, the working ORP sensor was swapped over from the TMC to the conventional rosette for the corresponding deep casts (ORP-07). The TMC rosette was run by a Teflon cable with an operational depth limit of 2000 m and a wire out/in speed of 30 m/min. Tension limits restricted TMC operations to wave heights of up to about 8 – 9 feet, and operations were thus hampered on several days throughout the duration of the cruise. The

conventional CTD was running with a wire out/in rate of 50 m min^{-1} with a standard conducting hydrowire. Both CTD rosettes were equipment with an altimeter. The TMC rosette was either lowered to 10 m above seafloor (in waters <2000 m) or to a maximum depth of 2000 m. The conventional CTD went most often to 200 m. In some cases, when not over the ridge or over a seamount, it only went to 2000 m even with a few hundred meters more to go to the seafloor.

TMC sampling requires bottle preparation and sampling procedures different from conventional CTD sampling. During transit and at the first few stations of the grid, two soak casts were executed to condition both the OTE and the GO-FLO bottles. Then, before each TMC cast, all bottles were carried out of either the TMC van or the TMC bubble and mounted on the TMC rosette. Each open bottle was protected from outside dirt by a shower cap arranged over the open top of the bottle. Once the bottles were mounted on the frame, they were prepared for deployment. The shower caps were removed immediately before the CTD went into the water. Upon recovery, the shower caps were placed back on the bottles to cover their tops. Before carrying the bottles back into the TMC van or the bubble, gas sampling was performed. All other sampling was performed in either the TMC van or the bubble. After all bottles were removed, the CTD rosette was rinsed with fresh water. To allow somewhat cleaner samples from the conventional rosette, the traditional springs were replaced with Teflon springs before the first CTD cast. Subsequently, a bottle check cast was performed to determine the blank values for dFe analysis. When collecting clean samples from the conventional CTD, the CTD rosette package would be rinsed after sampling was completed.

Trace metal clean water samplers. Two different cast types were conducted using the TMC rosette: a 'full' cast using 10 L, General Oceanics, Teflon coated GO-FLO bottles with two Teflon petcocks that allowed for gas sampling; and a 'FIA' cast which deployed 10 L, Teflon coated, Ocean Test Equipment (OTE) Model 114 C-Free Chamber Water Samplers, with a single Teflon petcock. TMC Full casts were sampled for He and CH_4 on deck and then moved to the TMC van to sample for total dissolvable and dissolved metal, dissolved ligands, metallophores, dissolved Mn(III), dissolved and particulate Th, and total particulates. For TMC FIA casts, OTE bottles were moved directly into the wet lab bubble and sampled for all the constituents mentioned above, except for gasses. Shipboard FIA analysis of Fe from all bottles sampled from a single depth (St. 5, casts 3 and 4) found that all bottles had acceptable background concentrations, with one expectation, OTE bottle #4, which was regularly checked and eventually fell to an acceptable level. GO-FLO bottles operated well throughout the cruise, having only the occasional misfire or leaker – both malfunction types were noted on the cast sheet. The OTE bottles were another story entirely as they failed early, often, and randomly despite efforts to adjust and fine tune the ball valve assemblies. As a result, the OTE bottles were relegated to collecting surface waters for incubation experiments or bottles were double tripped at most depths during profile casts.

Shipboard observations from CTD casts. Shipboard observations based on the ORP and LSS sensors revealed two areas of special interest: A caldera with an ORP anomaly close to the seafloor first observed at St. 72 during the second pass of the grid, and a hydrothermally active area with large turbidity anomalies first observed at St. 82 during the second pass of the grid. Both areas were revisited after finishing the second pass of the grid. St. 111 confirmed the initial findings at St. 72 with a large ORP anomaly in the crater. Subsequently, a large flow and flux study was conducted with eight stations around the crater and a chemical study was conducted using two stations on the crater rim (St. 114, St. 117) and one on the flank (St. 116) of the volcano. Similarly, revisiting the area of St. 082, confirmed the presence of a large particle plume. A mini-grid was conducted (St. 124-146) to map out the extent of the observed plume. In addition to particle anomalies, St. 127, St. 134 and St. 135 also showed ORP anomalies and thus indicate a hydrothermal source in close proximity. St. 124 and St. 131 displayed a large particle

plume, 1.7 km think and reaching almost to the surface layers showing that deep hydrothermal activity can influence the surface ocean.

Pump casts. In addition to the TMC and conventional CTD casts, five pump casts were executed during this cruise. Pump casts delivered seawater directly into the TMC van using a PTFE Teflon diaphragm pump (Almatec A-15TTT) and a 50 m length of PFA tubing (½" OD, 3/8" ID) secured to a polyester braided line anchored by a 9 lb., powder-coated kettle bell. Pump casts were deployed off the starboard using the ship's A-frame. Line was lowered to 10 m and sampled after a 5-minute rinse. During sampling, the ship's bilge was secured and the propeller disengaged. Total and filtered seawater for incubation experiments were collected through a 1000 um Nitex mesh and from an inline 0.2 µm capsule Acropak-500 filter, respectively. Sample volumes were between 100 and 200 liters per deployment.

TMC spaces. The chemistry team utilized three TMC spaces aboard the ship: a bubble in the aft dry lab, a bubble in the wet lab, and a TMC van provided by USAP. The two bubbles were constructed with plastic sheeting provided by the ship. The bubble in the aft dry lab was the largest, taking up more than half of the lab. Positive pressure was maintained with two large HEPA filters and a laminar flow hood. Sample processing, incubation time points, acidification, and FIA were conducted in the aft dry lab bubble. Positive pressure in the wet lab bubble was maintained by two laminar flow hoods. Subsampling of the OTE bottles was conducted in the wet lab bubble. Sampling of the GO-FLO bottles was conducted in the USAP TMC van.

After gas sampling, bottles were carried to respective sampling locations and secured into racks. Elbows of rigid Teflon tubing were inserted into the sampling petcock, replacing a stopper that was in the petcocks during casts. Bottles were pressurized with 0.2 µm filtered air using an air manifold system similar to those used in past TMC sampling campaigns. Bottle fittings — including stoppers, elbows, and connections between the bottle and air system — were acid-washed as appropriate.

Once bottles were pressurized and fitted with sampling elbows, the chemistry team began the subsampling process. The sampling team was comprised of Buck, Monreal, Davis, Walker, and. Jenness. Samplers wore Tyvek gowns, plastic shoes, and bouffants during sampling. Subsampling was conducted in the style of past US GEOTRACES cruises. Bottles used for sampling each depth were staged in large plastic bags (one bag per GO-FLO or OTE bottle) and moved into sampling location prior to the CTD rosette coming on deck. Samplers would open each large bag with "dirty hands" and then commence sampling with "clean hands" using vinyl gloves.

Seawater was allowed to flush through the elbow for a few seconds and then a 30–125 mL unfiltered sample for total dissolvable trace metals (Barrett/Resing) was taken from the elbow. A 0.2 µm Acropak-200 Supor capsule was then connected to the sampling elbow with a 3 inch piece of acid-washed Masterflex L/S 24 tubing. Seawater was allowed to flush through the Acropak for a few seconds before filtered samples were collected.

The sampling sequence for a typical "Full" station was as follows. The first filtered sample was a 60–125 mL sample for FIA (Barrett/Resing), followed by a 60–125 mL sample for ICP-MS analysis (Bundy). These samples were collected in low-density polyethylene bottles. Following this, a 500 mL sample for iron-binding ligands (Bundy) was collected in a fluorinated high-density polyethylene (FLPE) bottle, and a 1 L sample for Mn(III) (Bundy) was collected in a polycarbonate bottle. All bottles were rinsed three times according to the GEOTRACES Cookbook. The last samples taken were for dissolved metallophores (Bundy) and particulate trace metals (Barrett/Resing). All 4 L or 8 L polycarbonate bottles were rinsed three times through the Acropak. Then, the polycarbonate bottles were set up to collect filtrate through a 0.2 µm polycarbonate filter in an acid-washed filter holder. Connections between the sample bottles, filter holders, and sampling elbows were comprised of acid-washed Masterflex 24 L/S or rigid

Teflon tubing. Some extra samples (e.g., Fe(II) at hydrothermal sources, biological parameters) were added when appropriate. At "FIA" stations, oftentimes only total dissolvable and dissolved trace metals samples were taken. See Table 5 for full breakdown of samples taken at each station.

Sampling time depended on the number and types of samples being taken at a particular station but ranged from 1 hour at pure "FIA" station and 4 hours at "Full" stations. After sampling was completed, volumes pushed through the polycarbonate filter were recorded, GO-FLO/OTE bottles were depressurized, and prepared for the next cast. Samples were run to the large bubble in the aft dry lab to be further processed, frozen, acidified, and/or stored.

Fig. 18. Vertical section of dFe along the KR1 ridge. Bathymetry: GEBCO Compilation Group (2024); dFe analysis by P. Barrett; map by N. Buck.

Shipboard dissolved Fe analysis
P. I.: Resing
At Sea: Barrett

Approximately 900 samples at 75 stations were analyzed for dFe using a modification of the shipboard flow-injection analytical technique of Measures et al. (1995). Water-column samples were collected using a TMC CTD-rosette and filtered through a 0.2 μm Acropak into clean 100 mL LDPE sample bottles prior to analysis. Shipboard measurements provided a check on potential contamination, facilitated adaptive sampling to locate hydrothermal sources and assess their downstream impacts on surface ocean dFe inventories, and informed sampling strategies of other parameters by other cruise participants. Filtered seawater samples collected will also be analyzed post cruise for dissolved manganese (dMn) at NOAA-PMEL.
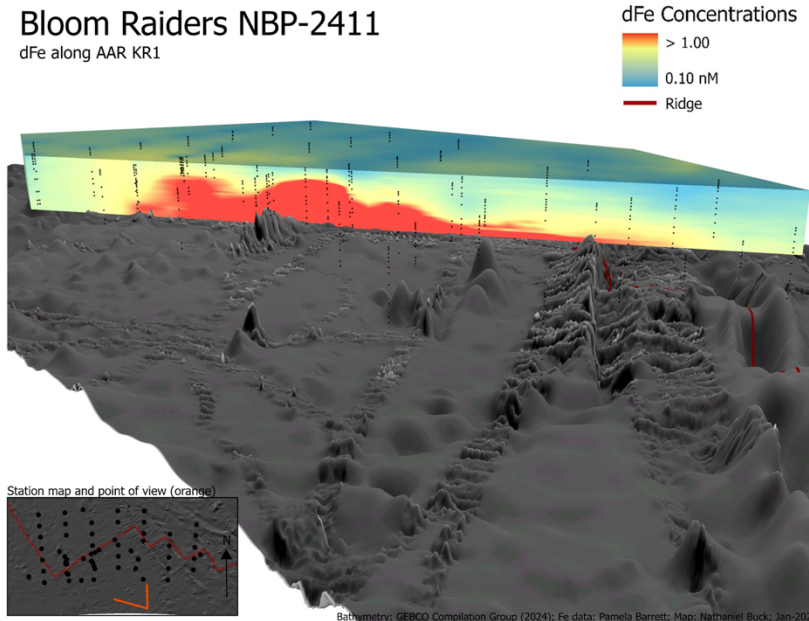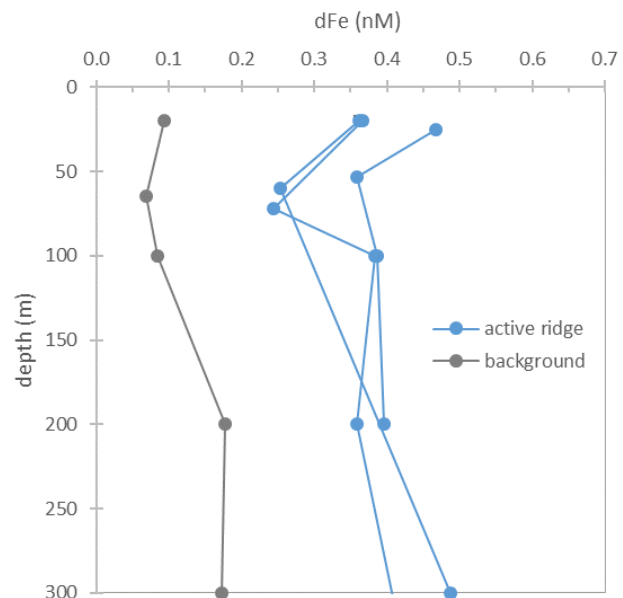

Fig. 19. Impact of hydrothermal Fe on surface ocean dissolved Fe (dFe) concentrations. Profiles of dFe in the upper 300 m at a background station and 3 stations over action sections of the ridge.

Preliminary results show that elevated dFe is coincident with strong LSS signals and ORP anomalies in the study area, indicating supply from hydrothermal activity, with high (>10 nM) concentrations measured at key stations along the ridge and at the seamount sampled at station 72 and 111–122 (Fig 18). Concentrations of dFe in the upper water column at these stations are elevated compared to background profiles in the study area (Fig 19), strongly indicating likely supply of hydrothermal Fe to the euphotic zone.

Total dissolvable metals (TM). Approximately 650 unfiltered seawater samples were collected into clean 100 mL LDPE bottles at 70 stations using a TMC CTD-rosette for post-cruise analysis of total dissolvable iron (TFe) and manganese (TMn) at NOAA-PMEL.

Particulate trace metals (pTM). Approximately 500 samples for post-cruise analysis of total particulate trace element (pTM) concentrations were collected at 45 stations. Total particulate matter was collected onto 37 mm, 0.2 µm pore polycarbonate track-etch membrane filters from seawater collected using a trace metal clean CTD-rosette. Total particulate trace element concentrations (Al, Si, P, Ca, Ti, V, Cr, Mn, Fe, Ni, Cu, Zn, and Pb) will be analyzed by energy-dispersive X-ray fluorescence (Buck et al., 2021) at NOAA-PMEL.

Table 5. Number of samples collected for shipboard dFe analysis, total dissolvable Fe and Mn (TM), particulate trace metals (pTM), dissolved thorium (dTh), particulate thorium (pTh), dissolved trace metals (dTM), Fe-binding ligands (dFeL), dissolved Fe siderophores (dSid), dissolved Mn(III) (dMnIII), dissolved Mn speciation (MnSpec), dissolved Fe(II) (dFe(II)), dissolved iron isotopes (dFe_Iso), and inorganic macronutrients (Nuts).

	Shipboard dFe	TM	pTM	dTh	pTh	dTM	dFeL	dSid	dMnIII	Mn Spec	dFe(II)	dFe _Iso	Nuts
Station	929	642	517	79	59	806	542	379	251	43	18	2	27
Incubation	0	0	0	0	0	355	117	36	0	210	0	0	0
Total	**929**	**642**	**517**	**79**	**59**	**1161**	**659**	**415**	**251**	**253**	**18**	**2**	**27**

Trace Metal Concentrations and Speciation
P. I.: Bundy, Resing
At-Sea: Buck, Monreal, Davis, Jenness

Dissolved trace metals (mass spectrometry). *Background*: In addition to Fe and Mn from shipboard and shoreside FIA by Resing and Barrett, dissolved trace metal samples were collected for inductively coupled plasma mass spectrometry (ICP-MS). Analyses via ICP-MS will provide concentrations for additional metals (e.g., cobalt, zinc, nickel, cadmium, etc.) as well as comparable concentrations for Fe and Mn, giving high confidence in measurements. Data for other metals will enhance interpretation of Fe sources and allow assessment of other limiting or potentially toxic trace elements for bloom formation.

Sampling: Samples for ICP-MS analysis were taken from all "Full" (GO-FLO bottles) trace metal casts and most "FIA" (OTE bottles) trace metal casts. When samples were taken, typically all depths were sampled. In sum, 806 environmental samples were collected via filtration of seawater from pressurized GO-FLO or OTE bottles through a 0.2-µm Acropak Supor (Pall) capsule filter into a 125 mL or 60 mL low-density polyethylene (LDPE) bottle. Additionally, 355 samples were collected from shipboard experiments into 60 mL LDPE bottles. Most samples were acidified shipboard to 0.024 M HCl for shoreside analysis. Three rinses were conducted

prior to filling each bottle, and all equipment for sampling including bottles had been acid-washed according to the GEOTRACES Cookbook. A small number (<20) of samples were taken from the conventional rosette in hydrothermal plume maxima, where concentrations with shipboard FIA were demonstrated to be high enough that contamination was likely negligible. Finally, two samples at potential sources were collected for iron isotope analysis.
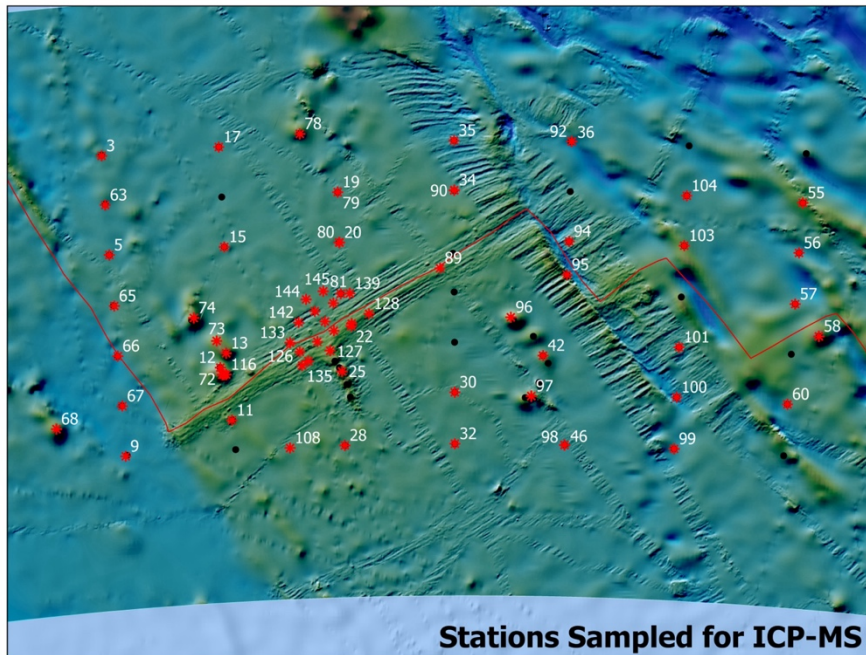

Fig. 20. Stations sampled for ICP-MS analysis.

Analysis: Acidified samples will be analyzed in the TraceLab at the University of Washington School of Oceanography. For elements with stable isotopes, an aliquot will be weighed and spiked with known isotopes and loaded into a SeaFAST system. In the SeaFAST system, aliquots will be buffered in-line to pH 6.3 with an Optima-grade ammonium acetate buffer, loaded onto a column fitted with Nobias-chelate PA1 resin, and rinsed with buffered ultrapure water to remove salts. Samples will then be back-eluted with 10% (v/v) Optima-grade nitric acid for analysis on an Element II ICP-MS. Monoisotopic elements like Mn will be quantified with a standard curve made with matrix-matched seawater collected from the surface Southern Ocean.

Samples near and downstream of hydrothermal sources will be prioritized for analysis.

Dissolved metal-binding ligand quantification (voltammetry). *Background*: Organic speciation parameters will provide several insights to the cruise objectives, such as assessing the stability of Fe from a particular source, describing the bioavailability of the Fe pool, understanding the surface community's response to Fe inputs, and even tracking an Fe source (e.g., terrestrial sources of iron are often associated with higher levels of humic-like ligands). Thus, in line with the hypothesis of the cruise, heavier sampling was conducted near sources like seamounts and hydrothermal plumes.

Sampling: Samples to determine the concentration and strength of the Fe-binding ligand pool were taken from all "Full" (GO-FLO bottles) TMC casts and some "FIA" (OTE bottles) TMC casts. When samples were taken, typically all depths were sampled. In sum, 542 environmental samples were collected via filtration of seawater from pressurized GO-FLO or OTE bottles through a 0.2-μm Acropak Supor capsule filter into a 500 mL fluorinated high-density polyethylene (FLPE) bottle. Additionally, 117 samples were collected from shipboard experiments. Bottles were frozen shipboard at -20°C. Three rinses were conducted prior to filling each bottle, and all equipment for sampling including bottles had been acid-washed according to the GEOTRACES Cookbook. A small number (<10) of samples were taken from the conventional rosette in hydrothermal plumes, where concentrations with shipboard FIA were demonstrated to be high enough that contamination was likely negligible.

Analysis: Frozen samples will be thawed and analyzed with voltametric titrations in the Bundy Lab at the University of Washington School of Oceanography. Specifically, competitive ligand exchange adsorptive cathodic stripping voltammetry (CLE-ACSV) with salicylaldoxime as the artificial ligand will be run on a BASi hanging mercury drop electrode with a platinum auxiliary electrode and Ag/AgCl reference electrode (Bioanalytical Systems Incorporated). Titrations will provide organic speciation parameters like dissolved Fe-binding ligand concentrations ($[L_1]_{Fe}$, $[L_2]_{Fe}$, etc.), binding strengths of the organic ligand pool ($\log K^{cond}_{FeL,Fe'}$), and free Fe concentrations ($[Fe`]$).

Fig. 21. Stations sampled for Fe-ligand analysis.

Samples near and downstream of hydrothermal sources will be prioritized for analysis. As samples are thawed, an aliquot will be poured off for dissolved nutrient analysis at the University of Washington as an additional GO-FLO and OTE bottle check for trace metal concentrations. Furthermore, samples can be used for organic copper speciation (determining copper toxicity) or humic-like ligand quantification with similar equipment if relevant to cruise objectives.

Metallophores and specific metal-organic complexes (mass spectrometry). *Background*: In addition to organic speciation of metals, samples were taken for the characterization of discrete strong-binding ligands (i.e., metallophores). From promoting dissolution of Fe from minerals to detoxifying free Cu ion, microbially-produced metallophores such as siderophores, serve an outsized role in complexation despite our limited knowledge of their dynamics, making their quantification in environmental samples of particular interest. In Fe-limited systems like mesopelagic waters or the surface of the Southern Ocean, siderophores can be the dominant ligand, controlling metal cycling and transport. Identifying and characterizing siderophores will thus be important understanding the fate and transport of metal from a source to the surface and how the surface community may recycle micronutrients to extend the duration of the AAR bloom. Siderophores have also been used as a signal of Fe-stress as evidence suggests that their production is highest under high nitrogen-to-iron ratios

For most environmental samples, 4.5 L of seawater was loaded onto columns, which is in line with recent sampling campaigns (4 L) for siderophores. When possible, 6–8 L of sample seawater was collected to provide higher sensitivity for key sources like hydrothermal vents. Recent work suggests that hydrothermal Fe may be stabilized for distal transport by strong ligands such as siderophores, and these large-volume samples may provide further insight to this preliminary evidence.

Sampling: Samples to determine metallophore concentrations and identities were taken from all "Full" (GO-FLO bottles) TMC casts and occasional "FIA" (OTE bottles) TMC casts. When
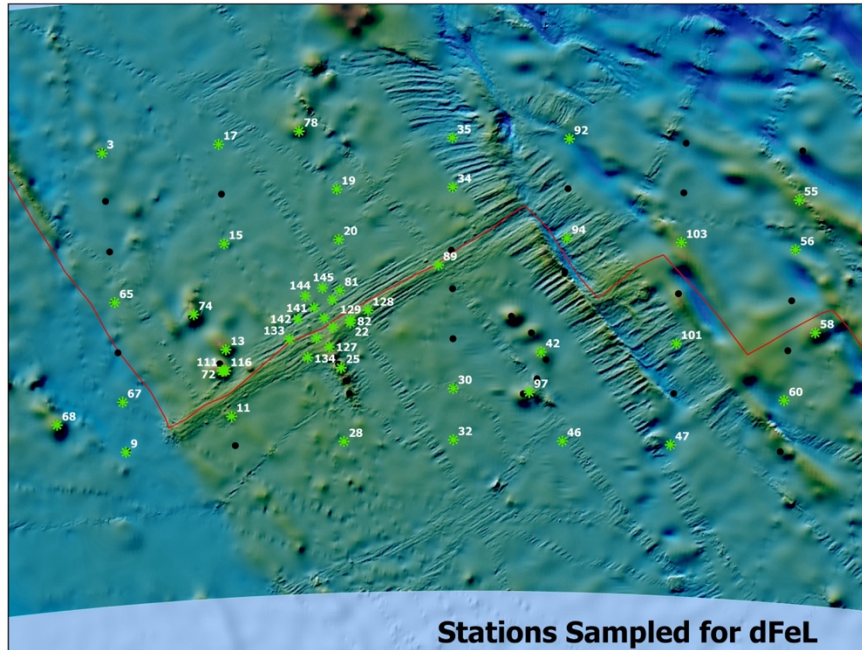
29

samples were taken, 8–10 depths were chosen. In sum, 379 environmental samples were collected via filtration of seawater from pressurized GO-FLO or OTE bottles through a 0.2-µm polycarbonate filter into a 4 L or 8 L polycarbonate bottle. Filters from this were collected by Barrett for particulate metal analysis. Additionally, 36 samples were collected from shipboard experiments. Three rinses were conducted through the 0.2-µm Acropak Supor capsule filter prior to setting up the

Fig. 22. Stations sampled for siderophores.

polycarbonate filter, and all equipment for sampling including bottles had been acid-washed according to the GEOTRACES Cookbook. A small number (< 10) of samples were taken from the conventional rosette in hydrothermal plumes, where concentrations with shipboard FIA were demonstrated to be high enough that contamination was likely negligible. Two samples were also *ultra-filtered* with a 10 kDa Pellicon cartridge to see if siderophores were in the soluble or colloidal phase.

After the polycarbonate bottles were filled with sample seawater, they were taken to the large HEPA-filtered bubble in the aft dry lab. Polystyrene divinyl benzene (Bond Elut ENV, Agilent Technologies) solid phase extraction columns with a 1 g bed size were activated with 10 mL of HPLC-grade methanol, rinsed with pH 2 Milli-Q water, and then rinsed with regular Milli-Q water. Filtrate was then slowly pumped onto SPE columns through acid-washed Teflon tubing. After all the filtrate was loaded onto SPE columns, columns were frozen shipboard at -20°C.

Analysis: Frozen samples will be thawed and analyzed using various types of mass spectrometry in the Bundy Lab at the University of Washington School of Oceanography. Material will be eluted off the columns into a 15 mL acid-washed centrifuge tube with 14 mL of Optima-grade methanol using a vacuum manifold. Then, samples will be dried down completely on a Speed-Vac concentrator and resuspended in 0.4 mL Milli-Q. Concentrate will then be run with liquid chromatography coupled to inductively coupled plasma mass spectrometry (LC-ICP-MS) and electrospray ionization mass spectrometry (LC-ESI-MS) to identify discrete metal-binding compounds.

Samples near and downstream of hydrothermal sources will be prioritized for analysis. Additionally, while the focus will be on characterizing strong Fe-binding compounds, this method collects data that can be used to identify chelators for other metals as well (copper, nickel, manganese, cobalt, etc.). Other metallophores can be analyzed if relevant to cruise objectives.

Quantifying redox speciation of bioactive metals. *Background:* Samples were collected to quantify the partitioning of dissolved Fe and Mn between differing oxidation states. The
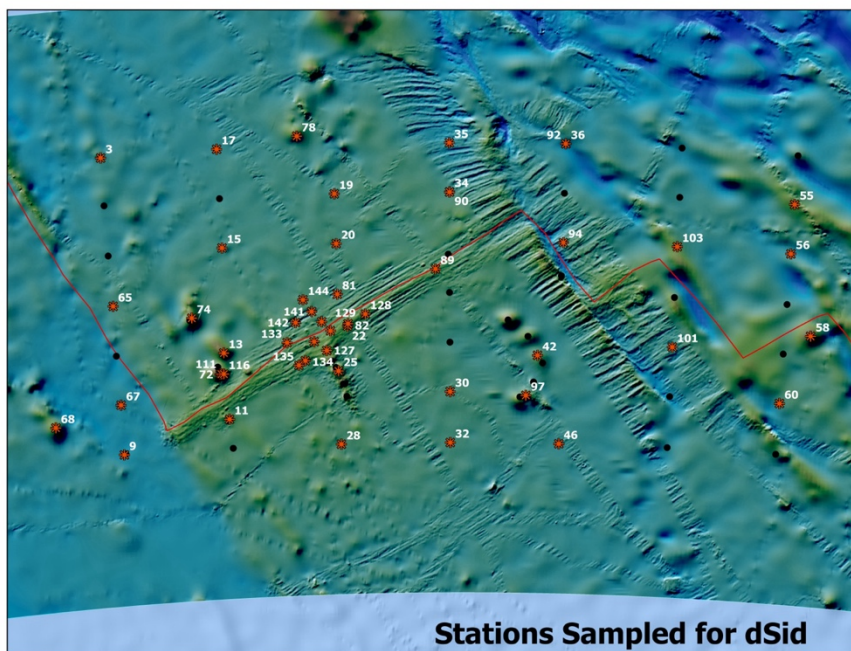
oxidation state of metals like Fe and Mn are key regulators of their bioavailability because, as far as we know, most bacterial and phytoplanktonic life only possess transporters to take up the most reduced form of each metal from seawater. For example, the two redox states of Fe that exist in seawater are Fe(II) and Fe(III). Considering that 99% or greater of dissolved Fe in seawater is Fe(III) bound to organic ligands, the main reservoir of Fe in seawater is not directly available to Fe transporters. Because hydrothermal vents are a source of Fe(II) to seawater, hydrothermal Fe may be fueling the AAR bloom, and Fe(II) is the most readily available form of Fe to phytoplankton, measuring Fe(II) in areas where there were LSS or ORP anomalies was of interest as a hydrothermal tracer.

Sampling: Two different types of samples to quantitatively fractionate redox speciation of Mn were taken during this research expedition, and they are differentiated internally in the Bundy lab as Mn(III) samples vs MnSpec samples. The most commonly-used techniques to quantify Mn speciation in seawater do not have detection limits low enough for the Southern Ocean (Thibault de Chanvalon and Luther, 2019; MnSpec samples), so Davis worked over this past summer to develop a method that is sensitive enough for Southern Ocean surface water (Mn(III) samples). Samples for Mn speciation were taken from most "Full" (GO-FLO bottles) trace metal casts and occasional "FIA" (OTE bottles) trace metal casts. When samples were taken, 4–12 depths were chosen. In total, 294 environmental samples were collected via filtration of seawater from pressurized GO-FLO or OTE bottles through a 0.2-µm Acropak Supor capsule filter into either 1 L or 4 L polycarbonate bottles (Mn(III) samples) or 30 mL LDPE bottles (MnSpec samples). Additionally, 210 samples were collected from incubation experiments via filtration of seawater through 0.2-µm Sartorius polycarbonate membrane filters into either 60 or 30 mL LDPE bottles (MnSpec samples). A small number of Fe(II) samples (18) were taken from hydrothermal stations with ORP anomalies and directly downstream of them. A small amount (<10) of samples were taken from the conventional rosette in hydrothermal plumes, where concentrations with shipboard FIA were demonstrated to be high enough that contamination was likely negligible. These samples were similarly filtered through a 0.2-µm Acropak Supor capsule filter into 30 mL LDPE bottles. Prior to filling, each bottle was rinsed 3x with filtered seawater. All equipment that encountered the sample was acid cleaned in accordance with the GEOTRACES cookbook.

After Fe speciation sample bottles were filled, they were immediately brought to the HEPA-filtered clean space in the aft dry lab and placed in a -20°C freezer. MnSpec samples were similarly immediately brought into the clean space upon filling the sample bottle and placed into the -20°C. Mn(III) samples were also taken to the clean space, where they were loaded onto monodisperse, N-vinylpyrrolidone-divinylbenze solid-phase extraction columns (Oasis HLB, Waters™) with a 200 mg bed space that had been activated with 8 mL of pH 7.8 HEPES (Millipore Sigma). Filtrate was loaded onto columns through acid-washed Teflon tubing at a flow rate of approximately 10 mL min^{-1}. Once all the filtrate was loaded onto the column, SPE columns were frozen shipboard at -20°C.

Analysis: Frozen metal speciation samples will be thawed and analyzed with UV-Visible spectrophotometry in the Bundy Lab at the University of Washington School of Oceanography. For Mn(III) samples, a modified method of Jones et al. (2019) will be used, whereby material will be eluted off the columns into a 15 mL acid-washed centrifuge tube with 14 mL of Optima-grade methanol using a vacuum manifold. Then, samples will be dried down to approximately 500 µL using a Speed-Vac. Concentrate will then be amended with leucoberbelin blue dye, an analyte that is sensitive only to oxidized Mn. It forms a sharp peak at 623 nm as the dye is oxidized by Mn, and we will exploit this to quantify dissolved Mn(III) in our samples. MnSpec samples will be amended with a competitive porphyrin ligand, which exchanges with natural

Mn(III) ligands in our sample. The resultant Mn(III)-porphyrin complex forms a sharp peak at 468 nm which can be measured in a 100 cm LWCC cell via UV/VIS.

A modified version of the method established by Stookey (1970) will be used to measure Fe(II) and total dFe. Thawed samples will be acidified with concentrated HCl and amended with an ammonium acetate buffer and ferrozine, which forms a complex with Fe(II) and creates an absorbance peak at 562 nm. This will be measured in a

Fig. 23. Stations sampled for dissolved Mn(III).. Map does not include other Mn speciation samples.

spectrophotometer with a 10 cm quartz cuvette. Samples will then be amended with hydroxylamine hydrochloride and equilibrated to reduce all dFe to Fe(II), allowing for a second absorbance measurement to calculate total dFe.

Dissolved Thorium

P. I.: Bundy
Cruise participant: Walker
With: Pavia

Background: Wind-blown mineral dust deposition provides a unique source of micronutrients to remote ocean regions, acting as a regulator of global biogeochemistry. In particular, dust deposition provides a source of Fe to the surface ocean – a key limiting nutrient in the Southern Ocean. Dust fluxes are especially low in the Southern Ocean, but observational data on Southern Ocean dust flux is limited. It is important to quantify dust fluxes in the AAR Bloom region because dust is one source of Fe to consider in our study's guiding question of what is driving the AAR bloom. Although we hypothesize dust flux to be low, quantifying it using long-lived thorium isotopes as a tracer will help constrain our understanding of global dust deposition and will improve future dust models.

Sampling: Samples to determine dissolved thorium concentrations were collected from both the GO-FLO bottles or OTE bottles at the same depths that dFe samples (FIA or ICP-MS) were collected. Typically, 6-8 samples from the upper 1000 m were collected at each station. There were issues with misfires on the OTE bottles, so some stations are missing more depths than anticipated. 79 dissolved thorium samples were collected at 10 stations across the grid (Fig. 24). Stations were chosen to capture a range of latitudes and were ultimately based on water availability.

After returning to deck, GO-FLO/OTE bottles were transported to the clean van (GO-FLO) or the clean bubble (OTE). dFe samples were collected first, and then the bottles were
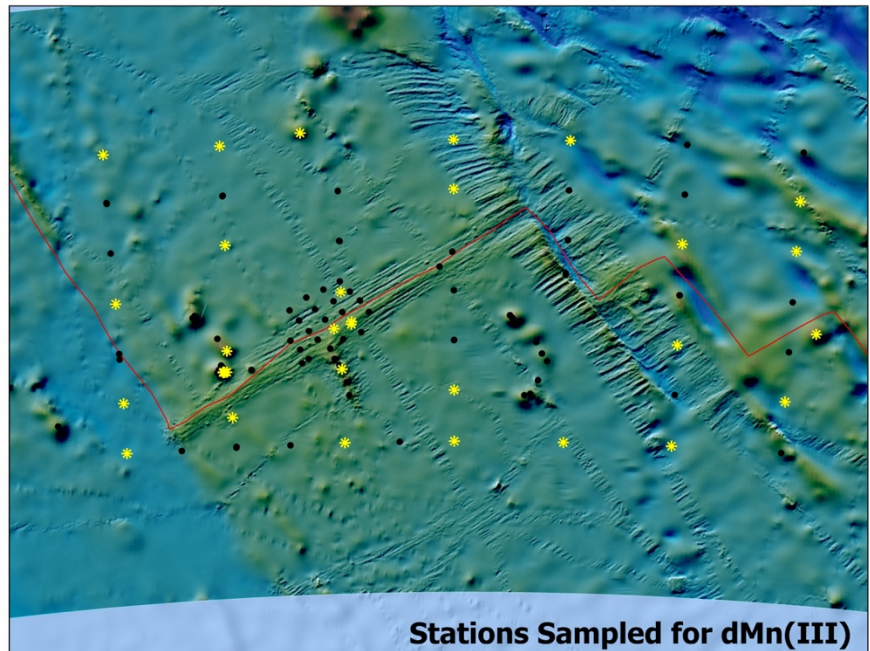
pressurized. Acid-clean Tygon tubing attached to both the top and bottom of an acid-cleaned 0.45 µm Acropak was attached to the GO-FLO/OTE nozzle and water was run through the Acropak for approximately 30 seconds. The acid-clean 3 L cubitainer was rinsed twice with 100-200 mL of seawater, and then filled to 90% capacity and the cap replaced. Afterwards, the cubitainer was placed on a flat surface, dried with a Kimwipe, parafilmed around the cap, the cap pushed back in so it was flush with the cubitainer, and the cubitainer was double bagged into Uline Ziploc bags. After all cubitainers were filled, the Acropak was emptied, double bagged, and placed into the fridge.

   Analysis: Cubitainers will be shipped back to the University of Washington where they will be promptly acidified with 5 mL of concentrated (12 M) Optima-grade HCl. ^{230}Th and ^{232}Th isotopes will be measured by isotope dilution using a Thermo ELEMENT XR ICP-MS. These measurements will be paired with the iron measurements taken at the same depths as dissolved thorium samples to create a 1-D mass budget and quantify dust deposition. The timeline of this analysis is unknown due to a lack of funding. Dr. Frank Pavia and Dr. Bundy plan to submit a proposal to run these samples.

Particulate Thorium
P. I.: Bundy
At Sea: Walker
With: Pavia

   Background:
Quantifying particulate organic carbon (POC) export flux is important to understanding the strength of the biological pump by determining the sinking rates of organic matter. Although we did not see an active bloom on NBP24-11, having POC flux estimates will still contribute to our understanding of the Southern Ocean biological pump. One way to determine POC flux is by using thorium isotopes. ^{230}Th is produced at a constant rate in the ocean by ^{234}U decay. ^{230}Th is

Fig. 24. Station map of dissolved and particulate thorium samples.

insoluble in the water column, and so it rapidly adsorbs to particles. We will use the ^{230}Th normalization method detailed by Pavia et al. (2019) to calculate POC flux.

   Sampling: We collected 59 filtered samples, for a total of 24 POC flux data points across the sampling grid. This includes four stations (Fig. 24) with six depths per station. Stations were chosen to reflect a range of latitudes and longitudes across the grid. Two casts were completed at each particulate thorium station, a surface cast (25, 50, and 100 m) and a deep cast (300, 600, and 1000 m). Samples in the surface were collected using the OTE bottles and analyzed in the
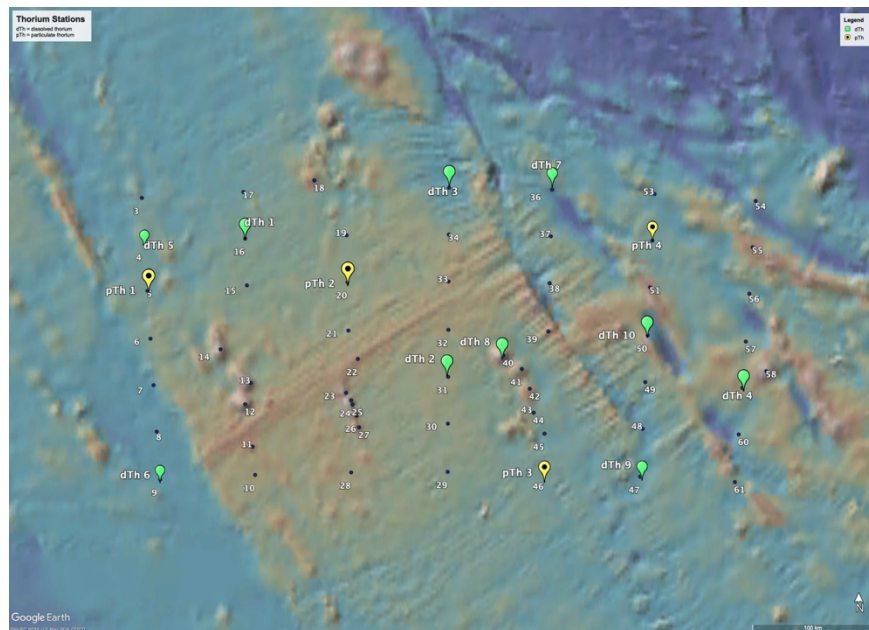
trace metal clean bubble. Samples in the deep were collected using GO-FLO bottles and analyzed in the trace metal clean van. Four bottles were fired at each target depth to constitute approximately 40 L filtered at each depth.

First, a dissolved trace metal sample (ICP-MS and/or FIA) and a 2.2 L POC sample were collected from one bottle at each depth. These samples will be analyzed following the relevant methods detailed in this cruise report. Next, an acid-clean filter holder containing an acid-cleaned Pall Supor800 0.8-µm polyethersulfone filter was connected to acid-cleaned Tygon tubing connected to the GO-FLO/OTE bottle. The bottle was pressurized and then water was filtered into a 10 L jerry can (graduated every 0.5 L). After the bottle was empty, the volume filtered was recorded, and the filter holder was hooked up to the next bottle at the same depth. If the flow rate was significantly slowed, as was the case with surface samples, a new filter holder was connected to the next GO-FLO/OTE bottle. The filter holder number, filter ID, and volume filtered through each filter was recorded. After sample collection, the filter holders were brought into the dry clean bubble. Filters were removed with acid-clean tweezers and placed into petri dishes labeled with the filter ID. Petri dishes were placed ajar in the dessicator to let the filtered samples dry out. Once dry, samples were wrapped and packaged.

Analysis: Filters will be shipped back to the University of Washington where they will be processed according to the ^{230}Th normalization method (Pavia et al. 2019). These measurements will be paired with the POC measurements, and statistical analysis will be performed to fit a b value to each POC flux curve. The timeline of this analysis is unknown due to a lack of funding. Dr. Frank Pavia and Dr. Bundy plan to submit a proposal to run these samples.

Dissolved Gases Helium and Methane
P. I.: Baumberger
At Sea: Baumberger

Sample collection and shore-based analysis for helium (He) isotopes. In total, 723 samples from 77 stations for shore-based He isotope analysis were collected during this cruise (Table 6). Samples for He were collected from the TMC CTD casts with GO-FLO bottles and from the conventional CTD. No samples were collected from the TMC OTE bottles. For TMC sampling, TMC tubing was used to connect the upper Teflon petcock of the GO-FLO bottles (rigid Teflon tubing to soft Teflon tubing) to the 'dirty side' of the He sampling (soft Teflon tubing with quick connect). Immediately upon recovery of the underwater sampling package, air-free water samples were flushed through 24 inch sections of refrigeration grade Cu tubing with duplicate half-sections and cold-weld sealed (crimper 'Champ') for later laboratory determinations of He concentrations and isotope ratios. Water samples for He were always first in the sampling hierarchy.

These samples will be analyzed in the Helium Isotope Laboratory at NOAA Pacific Marine Environmental Laboratory and Oregon State University in Newport, Oregon. Analysis will be performed by using a 21 cm radius, dual-collector, sector-type mass spectrometer specially designed for helium isotope analysis. The measurements are standardized using marine air and, if necessary, a precisely known geothermal standard (MM gas from Yellowstone Park, 16.5 Ra).

The first data batch of about 200 sample analysis will be expected by the end of 2025 with more analysis following shortly thereafter. Initial analysis will be focused on the area of the big particle plume, following by the caldera and then by a representative sample number of the grid.

Sample collection and shore-based analysis for dissolved methane (CH$_4$) concentrations. In total, 685 samples from 66 stations for shore-based dissolved CH$_4$ concentration analysis were collected during this cruise (Table 6). Identical to the He samples, they were drawn from the TMC GO-FLO bottles and the conventional CTD, but not from the TMC OTE bottles. CH$_4$

sampling always followed second in line, right after the He sample was drawn. TMC sampling was ensured by using a designated tube with rigid Teflon end to connect to the upper valve of the GO-FLO bottle. The water samples for CH_4 analysis were preserved in 125 ml glass serum bottles (Wheaton), poisoned with 0.5 ml 6 M NaOH using a pipettor application, and sealed with a blue butyl rubber stopper and an aluminum crimp-seal.

These preserved samples will be analyzed by headspace extraction and gas chromatography in the NOAA PMEL Butterfield laboratory in Seattle, WA.

The first data can be expected by the end of calendar year 2025. The priority list will be assembled according to the priority of He analysis as the CH_4 data will support the He data and help with further interpretations of source and fate of dissolved hydrothermal gases in the water column.

Table 6. Number of dissolved gas samples collected for helium (He), methane (CH_4), and dissolved inorganic carbon (DIC).

	He	CH_4	DIC
Stations	723	685	112
Incubations	0	0	0
Total	**723**	**685**	**112**

Dissolved Inorganic Carbon
P. I.: Bundy
At Sea: Walker

Background: Dissolved inorganic carbon (DIC) is the sum of the concentrations of carbonate, bicarbonate, and dissolved carbon dioxide (carbonic acid) in seawater. It is important for identifying where production is occurring (DIC drawdown) and where fresh hydrothermal activity may be occurring (elevated DIC). The DIC samples collected on NBP24-11 can also be analyzed for total alkalinity, a measurement of the buffering capacity of seawater. In conjunction, these two variables can be used to determine all aspects of the carbonate system (pH, pCO_2, etc.). Three kinds of DIC sampling were completed on NBP24-11. DIC samples were collected in 1) the upper 200 m to characterize surface production and provide more accurate simulated in-situ production calculations, 2) areas of hydrothermal activity, 3) the entire water column to obtain a background with which to compare the regions with hydrothermal activity.

Sampling: 112 DIC samples were collected (Fig. 25). Samples were collected in 500 mL borosilicate glass bottles. Before the cruise, bottles were heated in a muffle furnace at 450°C to eliminate any particulates or carbon compounds that may be contaminating the inside of the bottle. DIC samples were collected first from the conventional rosette because they are highly sensitive to gas exchange, photosynthesis, and respiration. If He and CH_4 samples were collected as well, DIC sampling would occur after these two gases. Nitrile gloves were worn throughout the entire collection process. Upon collection, tubing was inserted onto the Niskin bottle nozzle and flow was started. The tubing was flushed for ~30 seconds and bubbles were removed from the tubing. The DIC bottle was then opened and briefly rinsed upside down, which also rinsed the outside of the tubing. The tubing was inserted into the bottle of the bottle, and the bottle was overflowed twice. Approximately 5 mL of headspace was left in the bottle and the bottle was capped. After all samples were collected, the bottles were promptly brought back into the aft dry

lab. Nitrile gloves and goggles were worn. First, the stopper was removed and dried with a Kimwipe. The inside of the bottle neck was also dried, with care taken to not touch the Kimwipe to the sample. The stopper was then greased all around with Apiezon L grease in a zigzag pattern. To poison any biology that could contaminate the sample through production or respiration, 200 µL of saturated mercuric chloride solution was pipetted into the sample, with care taken not to touch the pipette tip to the sample.

Fig. 25. Station map of DIC. Hydrothermal sample stations are notated (HT), and deep stations are notated (Deep).

The stopper was inserted and turned around three times to create a seal with the grease. The bottle was then inverted five times to mix the mercuric chloride. It was then rubber-banded shut and stored in a cool, dry container.

Analysis: Samples will be shipped back to the Pacific Marine Environmental Laboratory where they will be analyzed using a DIC titrator and a total alkalinity titrator. The timeline of analysis is unknown due to funding constraints.

Experiments

DFe and 200 m Water Mixing Experiments
P.I.: Kevin Arrigo
At Sea: James Lauer
With: Gert van Dijken, Ali Palm, Sicada Sloan, Jenny Jackson, Cara Askren

Our objectives for this experiment were to evaluate the Fe limitation status of phytoplankton inside and outside the AAR bloom and to determine if dFe from a non-surface enriched water mass can stimulate surface production.

Method: Nine bioassays were conducted at stations throughout the study region in which surface water containing phytoplankton was mixed with filtered surface water (Control), filtered surface water amended with dFe (+dFe), and filtered water from 200 m or deeper (subthermocline) at the station where the surface sample was collected. Surface water was collected from 10 m either using either a TMC surface pump or the TMC CTD rosette, and water from 200 m or deeper was collected from the TMC CTD rosette. Unfiltered surface water was prescreened with a 1000 µm Nitex mesh to ensure large grazers, such as salps and copepods, were excluded without excluding large phytoplankton colonies, such as those formed by *Phaeocystis antarctica*, previously observed in the region. All filtered surface water and subthermocline water was filtered upon collection using 0.2 µm Acropak-200 Supor Capsule filters.
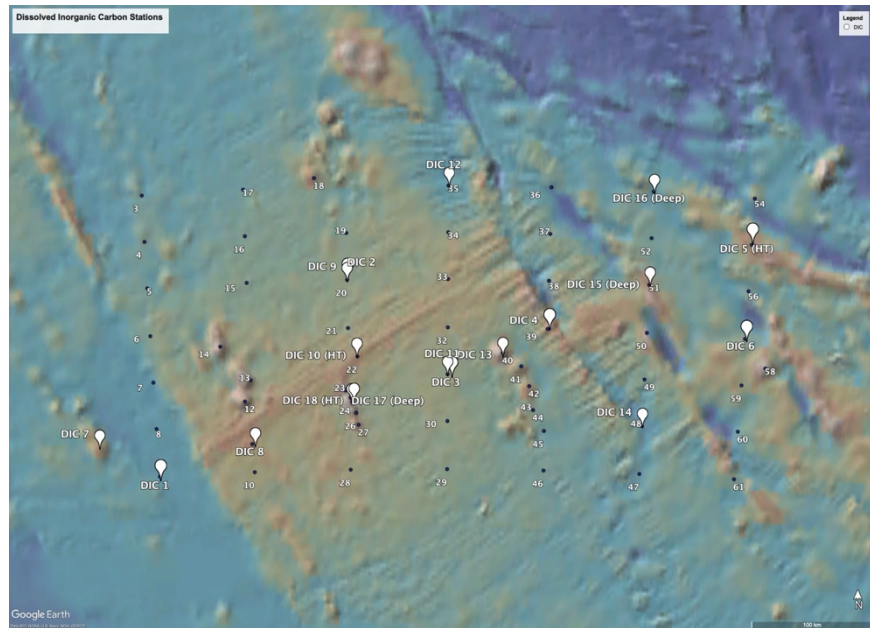
Control, regional, and dFe-amended water mixtures were prepared in two 50 L carboys, then dispensed into 21 two-liter clear polycarbonate bottles. Six bottles were prepared for each treatment, so that each could be sampled in triplicate at two time points: day 4 (96 hours) and day 7-10 (168-240 hours). Three additional bottles were filled with the control mixture and spiked with ^{13}C-labelled sodium bicarbonate (99%, Cambridge Isotope Laboratories, Inc.) and ^{15}N-labeled sodium nitrate (98%+, Cambridge Isotope Laboratories, Inc.) at 5% ambient DIC (2500 µM) and 10% ambient nitrate concentrations (30 µM), respectively, to assess initial phytoplankton production and nitrate uptake rates. The control and +dFe mixtures were prepared in the same carboy, as both contain a mixture of filtered and unfiltered surface water. After being dispensed into bottles, FeCl$_3$ dissolved in 0.2% HCl was added to the +dFe treatment to a final concentration of either 0.5 nM (experiments 1-3) or 5 nM (experiments 4-9). Bottles were placed in either on-deck incubators cooled with ambient seawater and screened to 50% incident PAR (experiments 1-5) or in an incubator van with a set temperature of 2°C where they received ~100 µmol photons m^2 s^{-1} incident PAR for 24 hours per day (experiments 6-9).

Each carboy was sampled for initial micronutrient concentrations, Chl a concentration, POC/PON, phytoplankton community composition (PlanktoScope), and characterization of algal physiology (labSTAF). This full suite of analyses was also taken in triplicate for each treatment at day 4 and day 7-10 of the experiment. Samples for dFe concentration were taken from carboys on day 0 and from all two-liter bottles at the final time point (D7-D10). All bottles sampled at the final time point were spiked 24 hours prior to sampling with ^{13}C-labelled sodium bicarbonate and ^{15}N-labeled sodium nitrate at the same concentrations (5 and 10% of ambient, respectively) to measure primary production and nitrate uptake rates over the final 24 hours of the experiment.

All culture vessels (carboys and bottles) were soaked for three days pre-cruise in 10% HCl, then three days in 1% HCl and stored in a small amount of 1% HCl during shipment and transit. All bottles were rinsed with Milli-Q water and with seawater from the sample mix prior to use. After each experiment, bottles were washed with 1% HCl then rinsed three times with Milli-Q prior to use again, and bottles and carboys were always used for the same treatments and mixtures.

Most samples from these experiments will be processed after the cruise, with only Chl a concentration and labSTAF data available shipboard. Preliminary analyses of Chl a data indicate that dFe amendment significantly increased Chl

Fig. 26. Panels A and B are Experiment 6 Chl a and Fv/Fm, Panels C and D are Experiment 9 Chl a and Fv/Fm. "Regional" indicates deep water collected at the station where the experiment was started.

a concentration relative to the control treatment in five of nine experiments conducted (Fig. 26). Bottles amended with subthermocline water had significantly higher Chl a concentration than the
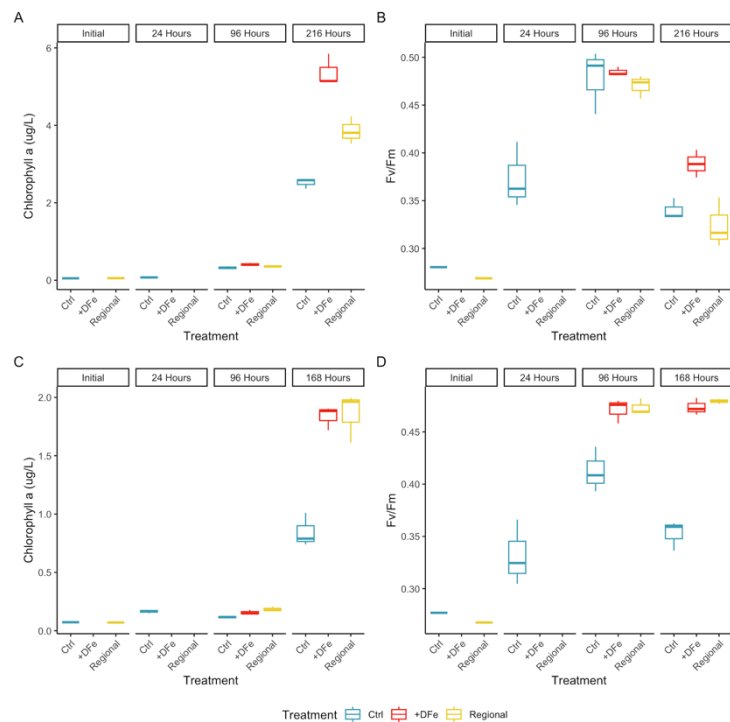
control group in three of nine experiments conducted and significantly lower Chl *a* concentration than the control in two experiments. DFe concentration in subthermocline water varied widely between stations at which experiments were started, and both experiments started at stations in which regional waters were enriched in hydrothermal dFe (experiment 6 and experiment 9) show significant increases in Chl *a* in the subthermocline water treatment, relative to the control (Fig. 26). Preliminary analysis of labSTAF data demonstrates that photosynthetic efficiency of photosystem II, as measured by the ratio of variable fluorescence (Fv) to maximum fluorescence (Fm), is enhanced with dFe amendment in four of nine experiments, particularly at the final time point. Fv/Fm is also enhanced in the subthermocline water treatment in three of nine experiments, and this enhancement of photosynthetic efficiency is consistent with relief of Fe limitation.

Oxidation of dissolved Mn in the presence of strong binding organic ligands

P. I..: Bundy
At-Sea: Jenness
With: Monreal, Davis, Walker

Background: In the Southern Ocean, Fe limitation leads to the microbial production of strong binding organic ligands, known as siderophores, to help acquire Fe. Certain siderophores have been shown to bind to dissolved Mn (dMn), stabilizing dMn in its +III oxidation state. An incubation experiment was conducted to understand how the presence of siderophores maintains Mn in the dissolved phase by preventing the oxidation of dissolved Mn to particulate Mn oxides, a process that forms Mn(III) as an intermediate, and how competition between Mn and Fe for binding to these siderophores influences the redox cycling and availability of Mn.

Protocol: At St. 92, a TMC cast using the OTE bottles was deployed to collect mixed layer seawater for this incubation and in situ measurements of total dissolvable trace metals (TdTMs), dissolved trace metals (dTMs; ICP-MS), dissolved manganese speciation (MnSpec), and particulate manganese oxides (MnOx; protocol below). At the same station, a second TMC cast using the GO-FLO bottles for environmental sampling was deployed, and mixed layer samples from this cast were utilized for in situ dissolved metallophores. Additional in situ measurements of inorganic nutrients and chlorophyll a were taken from environmental sampling of the mixed layer during a conventional CTD cast. Except for MnOx, for which no samples were collected outside of this incubation, all in situ sampling followed the same procedures as environmental sampling.

MnOx was measured using the method described by Altmann (1972) and utilized by Oldham et al. (2021). For in situ MnOx, 3.5 liters of unfiltered seawater was collected and filtered through a 0.2 μm polycarbonate track-etched membrane filter (Sartorius) on an acid cleaned Savillex filter rig. The filter was placed in an acid cleaned 15 mL polypropylene Falcon tube and amended with 3 mL of 0.0004% leucoberbelin blue dye (LBB), which reacts with MnOx and creates an absorbance peak at 623 nm. After allowing the filter to react with the LBB overnight, the filter was removed and remaining liquid was filtered through an Acrodisc 0.2 μm Supor Membrane syringe filter and injected into an LWCC 100 cm cell (World Precision Instruments), where the absorbance spectrum was measured using a UV-Vis spectrophotometer (Ocean Optics). A standard curve using synthesized MnO_2 will be used to convert absorbance measurements of samples to concentrations of MnOx.

The experiment was conducted in 36 acid-washed 1 L polycarbonate bottles. All bottles were filled with unfiltered mixed-layer water passed through a 1000 μm acid-washed Nitex mesh. Following collection, bottles were spiked with the following treatments to measure Mn oxidation

in the presence and absence of desferrioxamine, a siderophore known to bind to Mn and Fe, as well as in the presence of added Fe:

- Control
- + 5 nmol L^{-1} $MnCl_2$
- + 5 nmol L^{-1} $MnCl_2$, 2 nmol L^{-1} desferrioxamine mesylate (DFO; Sigma-Aldrich)
- + 5 nmol L^{-1} $MnCl_2$, 2 nmol L^{-1} DFO, 2 nmol L^{-1} $FeCl_3$

Following spiking, all bottles were sealed with Parafilm and electrical tape and placed in an outdoor incubator on the Helicopter Deck. The outdoor incubator was continuously filled with surface seawater and had a mesh cover to reduce light by approximately 50% to mimic light attenuation in the mixed layer. There were nine bottles for each treatment, with three of each budgeted per timepoint. Timepoints were taken on days 3, 8, and 14.

Timepoints: For each timepoint, three bottles of each treatment were collected from the outdoor incubator and brought to the HEPA-filtered bubble in the aft-dry lab. Unfiltered incubation water from the three replicates of each treatment was first collected in acid cleaned 60 or 30 mL LDPE bottles for TdTMs. The remaining water in the bottles was then filtered following the same protocol as the in situ MnOx. In order to reach the 2.7 nM detection limit of the MnOx method, the three bottles of each treatment were filtered one at a time through the same filter, with the filtrate being subsampled for dTMs and MnSpec before disposing the remaining filtrate and rinsing the filter rig with MilliQ water prior to the next replicate. On day 14, additional samples were taken to measure biological growth in the incubation period to address loss of metals to biology. Final inorganic nutrient samples were taken from the excess filtrate and Chl *a* samples were taken prior to filtration into 250 mL amber bottles and ran for each replicate of the four treatments in three 75 mL replicates.

Preliminary Results: Absorbances measured shipboard that correlate linearly with MnOx concentrations showed an increase across timepoints, with the treatment containing added Mn, Fe, and DFO exhibiting the highest concentration, and the treatment with added Mn and DFO exhibiting the lowest between treatments excluding the control. This begins to support the hypothesis that the presence of siderophores, and likely other Mn-binding ligands as suggested by Oldham et al. (2021), reduces oxidation of dMn to particulate MnOx. These results help explain the low concentrations of MnOx observed in the water column in the Southern Ocean (Oldham et al. 2021), which has broader implications for metal bioavailability, particularly as Mn is limiting or co-limiting to primary productivity in certain regions of the Southern Ocean (Browning et al. 2021).

Hydrothermal Mixing Experiment
P. I.: Bundy, Resing
At-Sea: Monreal

Background: While it is known that dFe can persist in hydrothermal plumes during distal transport, the bioavailability of dFe to the microbial community has not been investigated. We assessed the surface community's response to hydrothermal iron and the changes in iron speciation during plume mixing with a shipboard incubation that paralleled experiments conducted by Davis and Lauer. The plan at the start of the cruise was to collect water from a hydrothermal plume if one was discovered during environmental sampling and mix it in a manner similar to Lauer's bioassay with 200 m filtered seawater.

Protocol: At St. 82 along the KR1 ridge, a large hydrothermal plume was discovered between 500 m and 1200 m by the LSS sensor. This plume was later observed to take up the entirety of the water column when the site was reoccupied at the end of the cruise. During cast 4 at St. 82, four GO-FLO bottles on the TMC rosette were tripped at the plume maximum (900 m).

Environmental samples were collected for dissolved helium, methane, dissolved inorganic carbon, total dissolvable trace metals, dissolved trace metals (FIA and ICP-MS), dissolved iron-binding ligands, nutrients, dissolved manganese speciation, and dissolved metallophores. Then, 15 L was passed through a 0.2-μm Acropak Supor capsule filter into two acid-washed 8 L polycarbonate bottles. At St. 83, 10 GO-FLO bottles on the TMC rosette were tripped at 10 m. Similar samples were collected from these surface bottles, with the addition of standard biological parameters sampled by the Arrigo group and DNA filters collected by R. Moulton.

The experiment was conducted in 9 acid-washed 10 L polycarbonate carboys. For the
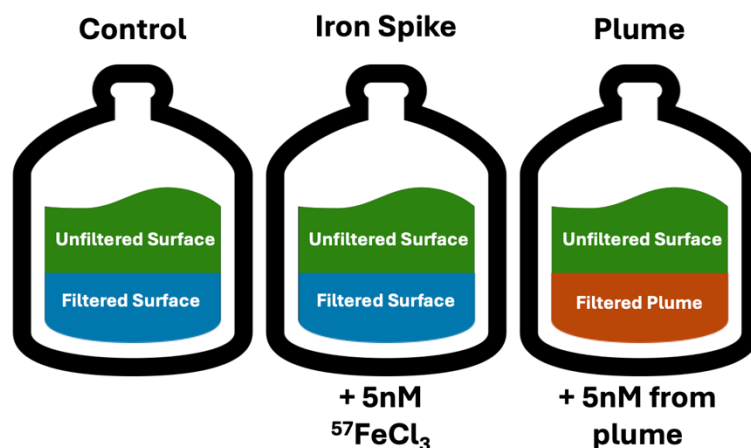

Fig. 27. Setup for the hydrothermal plume mixing experiment. Each treatment was conducted in triplicate.

controls, three carboys were filled with 5 L of filtered surface water and 5 L of unfiltered surface water. Unfiltered surface water was passed through a 1000-μm acid-washed Nitex mesh, and filtered surface water was passed through a 0.2 μm Acropak Supor capsule filter. For the plume treatments, three carboys were filled with 5 L of filtered plume water collected from St. 82 and 5 L of unfiltered surface water. To compare the plume treatments to a traditional iron spike, three carboys were filled like the controls (5 L filtered and 5 L unfiltered) but spiked with 5 nM $^{57}FeCl_3$. The spike level was chosen because shipboard FIA revealed the plume maximum to contain ~10 nM of dFe, so upon dilution, the plume treatment should have added ~ 5nM of hydrothermal dFe. Labelled iron will also allow measurement of uptake rate by tracking ^{57}Fe from the dissolved to particulate phases.

Thus, experiment consisted of three treatments: control, $FeCl_3$, and plume (Fig. 27). Carboys were incubated for 9 days in the incubation van provided by USAP. Subsamples were taken (T_1) immediately upon mixing, (T_2) on day 4, (T_3) on day 7, and finally (T_4) on day 9. Timepoints were chosen based on consistency with Davis and Lauer's experiments, as well as availability of the chemistry team during seamount and plume sampling campaigns at the end of the cruise.

During a timepoint, biological samples were poured off into amber bottles and handed off to the biology team, and chemistry samples were poured off into 1 L acid-washed polycarbonate bottles. Carboys were then immediately brought back into the van to limit exposure to lab light and temperature conditions. Water from the 1 L polycarbonate bottle was filtered through. A 0.2-μm polycarbonate filter mounted on an acid-washed Savillex Teflon vacuum rig. Filtrate was poured into bottles for dissolved trace metals (ICP-MS), dissolved manganese speciation, dissolved nutrients, and dFe-binding ligands. Remaining filtrate from triplicates was pooled into one metallophore sample per treatment. Filter was collected as a particulate trace metal sample. All filtering took place in aft dry lab bubble and was conducted by Monreal, Jenness, Davis, and Walker.

Table 7. Samples taken at each timepoint for the hydrothermal mixing experiment.

	In-situ plume	*In-situ* surface	Day 1 (*mix*)	Day 4	Day 7	Day 9
dTMs	X	X	X	X	X	X
pTMs	X	X	X	X	X	X
dSids	X	X	X	X	X	X
dFeL	X	X	X	X	X	X
Mn speciation	X	X	X	X	X	X
Nutrients	X	X	X	X	X	X
Chl *a*		*	X	X	X	X
FRRF		*	X	X	X	X
POC		*	*			X
PlanktoScope		*	*			X
DNA		X				X

Samples shared with Lauer, who started similar incubation in parallel (50% biomass dilution and mixing with 200 m-300 m water).

Preliminary Results: Experiment was successful. By day 9, concentrations of Chl *a* in the FeCl$_3$ and plume treatments measured by the Arrigo group were nearly double that of the controls. There was no significant difference in Chl *a* between the FeCl$_3$ and plume treatments, demonstrating that hydrothermally-derived dFe was relatively bioavailable to primary producers, (inorganic free dFe from an FeCl$_3$ stock is highly available if it remains dissolved). However, photosynthetic efficiency, represented by Fv/Fm, was significantly higher for the plume treatment relative to FeCl$_3$ at the end of the experiment, suggesting a higher degree of iron stress in the FeCl$_3$ treatment by Day 9. We hypothesize that either the dFe in the plume water was more stable and more easily recycled by the phytoplankton in the incubation, that another micronutrient in the plume treatment (e.g., Mn) aided growth, and/or that the type of iron selected for different communities. Shoreside trace metal, organic speciation, and genomic analyses will aid with interpretation.

This experiment is extremely important to cruise objectives, as the plume that was collected for this experiment was later found to take up the entirety of the water column, potentially reaching the surface. The changes in iron speciation (and therefore bioavailability) as plume water mixes with the surface should be observed through the measurements taken in this incubation. Furthermore, comparing ligand production in response to the mixing of plume water

in the incubation with the ligand composition of surface waters found over the ridge at the end of the cruise may yield important inside into how Southern Ocean phytoplankton respond to hydrothermal iron inputs.

Metal Addition Experiments

P. I: Bundy, Resing
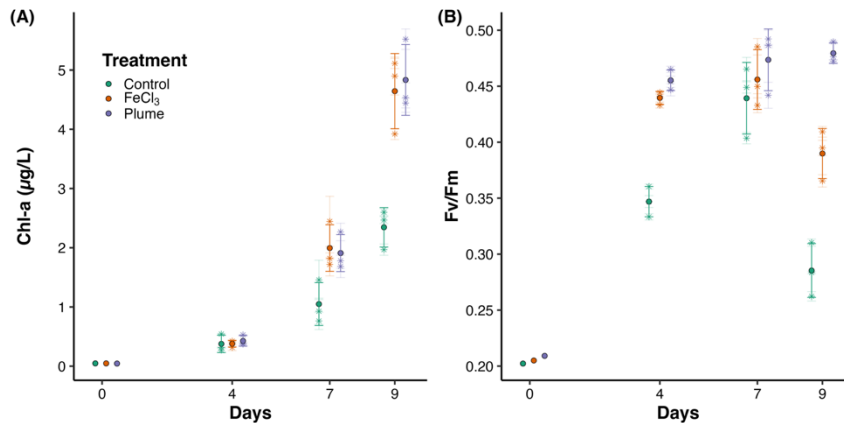At sea: Davis, Monreal, Moulton, Lauer, Jenness, Walker

Fig. 28. Chl *a* and Fv/Fm from the hydrothermal mixing experiment. Asterisks represent each incubation bottle, while points are the average of the triplicates for each treatment. Solid error bars represent one standard deviation of the triplicate incubation bottles, while transparent error bars are a standard deviation of each individual measurement.

Background: It is well known and well-characterized that the Southern Ocean is a high nutrient-low chlorophyll (HNLC) ocean basin whose primary production is most commonly limited by low Fe concentrations in surface waters. More recently, however, it has been shown that manganese (Mn) is the primary and/or co-limiting nutrient in certain areas of the Drake Passage, and follow-up modelling efforts revealed that Mn could potentially limit primary production in large swaths of the SO during austral spring/summer. This finding is unusual, as the typical open ocean profile of dissolved Mn contains a surface maximum. We hypothesize that Mn limitation in the SO could be due to the high percentage of the dissolved Mn pool that is bound to organics in surface (Oldham et al. 2021). To investigate the dynamics of differing metal limitations within surface waters of our study area, we conducted classic metal addition incubation experiments that paralleled experiments conducted by Monreal and Lauer.

Protocol: We will first describe the general set-up used for all four of the metal addition experiments. Surface water collected from 10 m was passed through a 1000 µm acid-washed Nitex mesh to remove large grazers and used to fill 4 L polycarbonate bottles that had been acid-cleaned according to the GEOTRACES cookbook protocol and triple rinsed with said surface seawater. In-situ samples were collected for Chl *a* concentration, photosynthetic efficiency, PlanktoScope,16S/18S DNA, dissolved trace metals (ICP-MS), dissolved metal-binding ligand quantification, labile particulate metals, dissolved Mn speciation, dissolved metallophores, and nutrients. Generally, fifteen 4 L PC bottles were filled to a total volume of 4.5 L for each experimental run, and each experiment consisted of five treatments:

- Control (no metal addition, only surface seawater passed through Nitex mesh)
- Surface seawater + 5 nM $FeCl_3$
- Surface seawater + 5 nM $MnCl_2$
- Surface seawater + 5 nM $MnCl_2$ and 5 nM $FeCl_3$
- Surface seawater + 5 nM Mn(III)-DFO

This spike level was chosen to be consistent with literature values used in the past in addition to tandem experiments occurring onboard alongside P. Monreal. Half of the experiments were spiked with labelled $^{57}FeCl_3$, which monitors Fe moving from dissolved to particulate phases and allows for the calculation of uptake rate (Table 8). Bottles were incubated anywhere from 8 to 10 days, depending on the amount of biomass that had grown throughout the experiment.

Subsamples were taken on day 4-7 (T_2), day 9-10 (T_3). Mid-experiment subsamplings (T_2), were scaled-down to conserve volume and assess biomass growth, and samples collected included Chl *a* concentration, photosynthetic efficiency, dissolved trace metals (ICP-MS), dissolved manganese speciation, and nutrients. Samples collected during experiment breakdowns (typically T_3) mirrored those taken at T_0, though a few select experiments were sampled for particulate organic carbon (POC) if volume allowed (Table 8).

During a timepoint, experiment bottles were collected from the incubation space and brought to the bubble in the aft dry lab. Biology samples (Chl *a*, FRRF, PlanktoScope, DNA, POC) were poured off first, then sufficient volume was filtered through a 0.2 μm polycarbonate filter mounted on an acid-cleaned Savillex Teflon vacuum rig. This filtrate was poured into single-rinsed LDPE sampling bottles for dissolved trace metals (ICP-MS), dissolved metal-binding ligands, dissolved manganese speciation, and dissolved nutrients. Sample bottles not in use were kept, to the best of the analysts' abilities, in a 4°C environment to limit time outside of a controlled environment. The filter was preserved in an acid-cleaned 2 mL LDPE microcentrifuge tube and frozen at -20 °C for later labile particulate trace metal analysis. All filtering took place in the after dry lab bubble and was conducted by Davis, Walker, Buck, Jenness, and Monreal.

The fourth and final experiment (METAD04) was conducted quite differently from the other three (Table 8). METAD04 bottles were incubated outside in the flowthrough deck incubators, thereby being exposed to ambient light and temperature conditions instead of the constant conditions of the incubation van. Additionally, personnel constraints limited the number of sub-samplings that we were able collect, so METAD04 consists of only T_0 and T_1 samples. In this instance, T_1 is representative of the breakdown timepoint and took place eight days after experiment set up. We also decided to omit the Mn(III)-DFO treatment from this experiment due to personnel and resource constraints. The water budget for this experiment was tight (S108C02 was shared with Lauer and a bottle misfired; the half of the bottles reserved for METAD04 had the misfire), so T_0 samples were collected from the leftover water in the surface bottle of S108C01. Though experiment water was collected at 10 m and the surface bottle was collected at 15 m, both depths were in the mixed layer. Therefore, we presume that T_0 samples from this water are sufficient to describe the conditions at 10 m.

Table 8. Experiment parameters for METAD01-METAD04

	Light van?	Length (days)	Fe Spike?	Mn(III)-DFO treatment?	Station number	Cast number	FRRF taken?	POC Taken?
METAD01	Yes	9	No	Yes	20	C3	No	No
METAD02	Yes	9	No	Yes	47	pump	Yes	No
METAD03	Yes	9	Yes	Yes	101	C2	Yes	Yes
META D04	No	8	Yes	No	108	C2	Yes	Yes

N₂ Fixation Rate Incubations and DNA/RNA Samples to Characterize N₂-fixing Community

P.I.: Arrigo
At Sea: Moulton
With: Turk-Kubo

The main objective of this experiment was to advance our understanding of the Southern Ocean's microbiome and establish an important baseline for N_2 fixation in this rapidly changing ecosystem.

Methods

Nitrogen fixation rate incubation experiments were performed using a $^{15}N_2$ gas tracer. Surface water was collected into nine 4 L bottles from the conventional rosette and, if necessary, the bottles were topped off with filtered seawater to ensure no atmospheric bubbles were present. 10 ccs of $^{15}N_2$ was injected into six 4 L bottles with Teflon-lined caps. The bottles were mixed and agitated for ≤15 minutes to distribute the $^{15}N_2$ tracer. After the $^{15}N_2$ bubble was released, the bottles were carefully topped off with 0.2 μm-filtered seawater to eliminate any atmospheric bubbles and moved to an onboard Percival model LT-41VL incubator. Three bottles were incubated for 24 hours at 300 μmol photons·m^{-2} s^{-1}, and the other three bottles were kept in the same incubator wrapped in black trash bags for dark incubations. The temperature of the incubator was adjusted to the sea surface temperature at the station where the water was collected. After the incubations were set up, triplicate T0s were broken down.

At T0 h, the bottles were subsampled for flow cytometry (FCM), DNA/RNA, POC/PON, and catalyzed reporter deposition-fluorescence in situ hybridization (CARD-FISH). To subsample for flow cytometry, 2 mL of seawater was added to pre-charged cryovials containing 20 μL of 20% glutaraldehyde. The cryovials were placed in miner bags at room temperature for ≥15 minutes, then flash-frozen and stored at -80 ℃. For DNA/RNA, 1 L from each bottle was added to acid-washed 2 L bottles and filtered using a peristaltic pump through 0.20 μm membrane disc filters. The filters were placed into sterile bead beater tubes, flash frozen, and stored at -80 ℃. For CARD-FISH, only one of the triplicate bottles was used. 95 mL was subsampled and added to an amber bottle containing 5 mL of sterile filtered 37% formaldehyde. The amber bottle was then stored at 4℃ for no longer than 48 hours and filtered onto a 0.6 μm polycarbonate filter. After filtering the 100 mL, the sample was placed into a cryovial and stored at -80 ℃. The remaining volume (>3 L) was used for POC/PON sampling, filtering as much as possible onto combusted GF/Fs. After sampling, the GF/Fs were stored at 60℃ in cryovials for 24 hours to dry, then capped and kept at room temperature.

After 24 hours, the light and dark bottles were subsampled for FCM, DNA/RNA, POC/PON, and CARD-FISH. Additionally, one of the light time points was used to subsample for membrane inlet mass spectrometry (MIMS). To subsample for MIMS, a peristaltic pump was used to pump water into a sterile 50 cc serum vial, overflowing the vial for >10 seconds. The septa to the vial were also filled with sample water and sealed using a crimper. The vial was inspected to ensure no air bubbles were present and stored at room temperature. Daily DNA/RNA and FCM samples were taken from 2 L bottles at six depths along with the nitrogen fixation rate experiments.

Results will be analyzed after samples are returned to the University of California, Santa Cruz for analysis.

Table 9. Summary of molecular sampling done during the NBP 24-11 cruise.

Parameter	Number of Samples
DNA/RNA	487
FCM	482
CARD-FISH	42
POC/PON	125
MIMS	16

Floats and Drifters

Floats

P. I.: Arrigo, Resing, Bundy, Baumberger
At Sea: Walker

Background: Argo floats are autonomous profiling floats that collect a profile every 10 days and transmit the data via satellite. Cruises of opportunity, such as NBP24-11, are critical for expanding the global Argo network. Seven core Argo floats and two deep Argo floats were deployed on NBP24-11 in coordination with Dr. Greg Johnson at the NOAA Pacific Marine Environmental Laboratory in Seattle, WA. Float deployment locations can be seen in Fig. 29.

Table 10. Float deployment information.

Date Deployed (GMT)	Time Deployed (GMT)	Lat (°S)	Lon (°E)	Serial #
12/18/2024	9:12	-61.000	155.484	7955
12/22/2024	8:11	-61.001	157.000	11690
12/28/2024	13:45	-61.745	159.982	7964
12/30/2024	12:32	-61.005	161.492	11691
1/1/2025	9:55	-62.999	162.985	7963
1/4/2025	5:42	-62.658	164.499	7947
1/8/2025	8:35	-62.999	155.498	11687
1/14/2025	21:25	-60.998	159.993	7948
1/19/2025	17:19	-61.000	162.996	7958
1/28/2025	6:40	-59.502	161.113	12102
1/29/2025	3:11	-56.803	164.140	12101

Float description: The core floats are S2-A MRV floats. They collect temperature, salinity, and pressure data up to 2000 m deep using a Sea-Bird SBE 41/41CP Argo CTD module. The deep floats are MRV Solo floats. They collect temperature, salinity, and pressure data up to 5000 m deep with the SBE 61 Deep Argo CTD. Data from the Argo floats can be visualized and accessed at the following link: https://dataselection.euro-argo.eu/

Drifters

P. I.: Arrigo
At Sea: Niu

Equipment and Techniques

A total of 18 drifters of two types were deployed during the cruise. 8 of the drifters are Surface Velocity Program (SVP) Drifters with 35cm sphere surface float connected with a cylindrical Holey sock drogue centered at 15m depth. This instrument is equipped with GPS-based tracking with accuracy of 2-50m (rms) and records Sea Surface Temperature (SST) with $\pm 0.05°C$ accuracy within the -5°C to 40°C sensing range at 5min intervals over their two-year lifespan. 10 other drifters are Surface Velocity Program Barometer (SVPB) Drifters with the same capabilities and an additional barometer on top of the surface float that measures sea level

pressure with ±0.4 hPa accuracy. Data is filtered out by an onboard algorithm before being transferred via Iridium Short Burst Data telemetry to the operators in 1 minute.

Deployment Information

Drifters are deployed either in pairs or in isolation at 12 stations (Table 11, Fig. 30). The first two pairs were deployed without detaching its magnetic pull trigger, which caused days to a weeklong delay in sensor activation by cold, near-freezing seawater.

Fig. 29. Map of Argo float deployment locations.

The rest 16 drifters were deployed after we manually pulled off the magnet trigger and ensured data transmission was successful an hour prior to deployment.
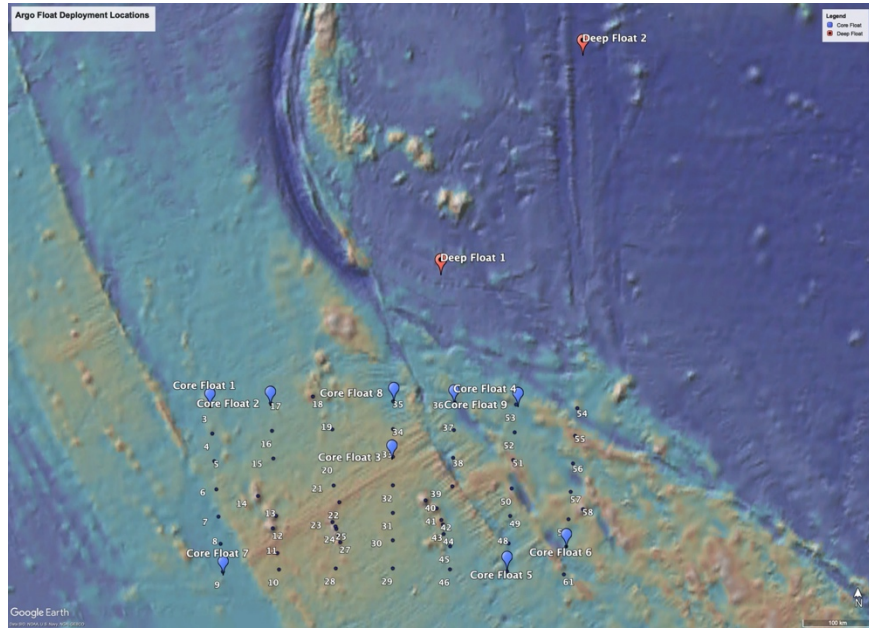
Study Design and Future Analysis

Drifter deployments were strategized around the following goals:

1) Characterize lateral dispersion rate of tracers in near surface water atop seamounts. We deployed drifters 1-4 in pairs for this purpose. We will estimate surface lateral dispersion rate based on the evolution of distance between a pair of two closely spaced drifters. Based on the barotropic nature of the flow, we will infer the dispersion rate at depths for these shallow seamounts.

Table 11. Drifter Deployment Documentation.

Drfiter Number in order of Deployment	Ship Name	Drifter ID #	Date	Time	Lat	Lon	Deployment from	Ship Speed (knots)	Height Above Mean Sea Level (m)	Station Number
1		300534065263750	25-Dec	14:42	-62° 26.7114'	158° 24.0262'	Stern and Port Side	5.8	3.35	23
2		300534065262820	25-Dec	14:42	-62° 26.7114'	158° 24.0262'	Stern and Port Side	5.8	3.35	23
3		300534065060030	25-Dec	18:20	-62° 29.1163'	158° 27.1153'	Stern and Port Side	2	3.35	24
4		300534064599710	25-Dec	18:20	-62° 29.1163'	158° 27.1153'	Stern and Port Side	2	3.35	24
5		300534065263730	2-Jan	17:07	-60° 59.9978'	164° 29.1923'	Stern and Port Side	2.7	3.35	54
6		300534065263810	2-Jan	17:07	-60° 59.9978'	164° 29.1923'	Stern and Port Side	2.7	3.35	54
7		300534065262790	3-Jan	19:11	-62° 11.7540'	164° 51.0261'	Stern and Port Side	2.1	3.35	58
8		300534065263800	3-Jan	19:11	-62° 11.7540'	164° 51.0261'	Stern and Port Side	2.1	3.35	58
9	Nathaniel B. Palmer	300534065261860	4-Jan	9:51	-62° 59.7305'	164° 29.9509'	Stern and Port Side	3.6	3.35	61
10		300534065262780	4-Jan	9:51	-62° 59.7305'	164° 29.9509'	Stern and Port Side	3.6	3.35	61
11		300534064699700	14-Jan	9:33	-61° 50.5358'	159° 34.5678'	Stern and Port Side	3.7	3.35	89
12		300534065262710	14-Jan	17:22	-61° 19.7928'	159° 59.8178'	Stern and Port Side	3.4	3.35	90
13		300534065060020	14-Jan	21:29	-60° 59.8954'	159° 59.5960'	Stern and Port Side	3.4	3.35	91
14		300534064599690	20-Jan	15:35	-62° 59.8887'	158° 29.7797'	Stern and Port Side	2.3	3.35	107
15		300534065262800	20-Jan	20:41	-63° 00.0086'	157° 44.7816'	Stern and Port Side	2.7	3.35	108
16		300534064599280	21-Jan	0:21	-62° 59.8879'	156° 59.8384'	Stern and Port Side	3.7	3.35	109
17		300534064599120	21-Jan	8:38	-62° 30.9236'	156° 52.7136'	Stern and Port Side	3.9	3.35	111
18		300534065060050	21-Jan	8:38	-62° 30.9236'	156° 52.7136'	Stern and Port Side	3.9	3.35	111

2) Characterize dispersion of surface water in near surface water within the phytoplankton bloom, north of the phytoplankton bloom (inside of the Antarctic Circumpolar Current), or south of the phytoplankton bloom (south of the ridge). Closely spaced drifter pairs will be used to characterize dispersion on smaller-scales. Drifters 5 and 6 were deployed within the ACC north of the bloom. Drifters 7 and 8 were deployed within the bloom, which is collocated with the front. Drifters 9 and 10 were deployed south of the bloom. The difference of surface flow evolution between the three pairs will inform us on the residence time of surface tracers and explain bloom locations.
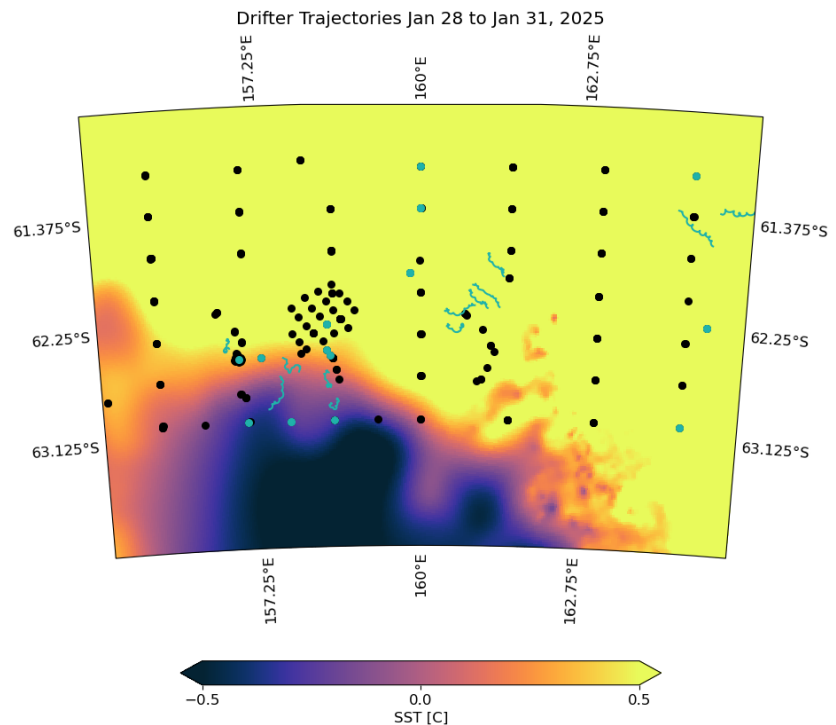

Fig. 30. Map of drifter deployment stations and drifter trajectories. Black dots indicate all our stations, and the blue dots mark the stations where we deployed drifters.

3) Characterize northward transport along a zonal transect at the southwestern end of the study radiator track and eastward transport at the north end of the grid. Drifters 14-16 were deployed along the zonal transect. We will use the drifter velocity averaging out near-inertial signals, combined with CTD density profiles, to calculate net zonal transport of the Balleny Gyre with the thermal wind balance. Another set of three drifters (11-13) were deployed along a north-south meridional line to capture variation of the gyre flow.

Outreach
P. I.: Arrigo
At Sea: Blount, Rawal

Polar STEAM, which stands for Science, Technology, Engineering, Arts, and Math, is an NSF-funded project that integrates and enhances two long-standing U.S. National Science Foundation (NSF) programs: the Polar Educators program and the Antarctic Artists and Writers program and facilitates virtual and deployment collaborations with scientists conducting research in polar regions. We had two Polar STEAM fellows accompany aboard our research cruise, an educator (Rawal) and an artist (Blount).

Objective. The primary goal as an outreach team was to communicate the science and life aboard the NBP 2411 expedition, focused on understanding phytoplankton blooms in the Australian Antarctic region of the Southern Ocean. This was achieved through a variety of mediums, including Instagram, Flickr, and blog posts. A secondary goal was to develop educational labs, lessons, and interdisciplinary projects to extend the impact of the research beyond the expedition.

Our Artist Fellow, Madeline Blount, engaged in several avenues of creative research onboard. She used the underway data to create an online interactive map, sharing the Palmer's location and progress with the public via a link on Instagram. She took thousands of digital photographs while on the ship using a Nikon Z9, documenting life onboard and science work, as well as studies of wave action and wildlife. A 180-600 mm telephoto lens was used for close-up photographs of multiple species of albatross, petrel, penguins, and whales. These photographs were regularly shared via Instagram, and available on the ship's public drive for those onboard to share with colleagues, friends, and family. Madeline used the Nikon Eclipse microscope and the attached SPOT sCMOS camera (color, 12 MP) to create darkfield images of phytoplankton and other organisms, supplementing the imagery from the lower-resolution PlanktoScope for aesthetic investigation and for public engagement. Rotating the phase condenser at the bottom of the microscope allowed for this dark and colorful background imagery style, at 4x and 10x magnifications. Madeline also began research on the current state-of-the-art machine learning techniques used to classify phytoplankton imagery datasets, beginning an investigation in the artistic potential of synthetic data generation for dataset augmentation, which will continue after the cruise.

Madeline also recorded sound throughout the ship, using a Zoom H1 digital recorder, as well as an Aquarian H2D hydrophone connected to a Zoom F3 field recorder. The sonic environment of the ship was recorded both in lab spaces and during three underwater drops from the main deck. The hydrophone was lowered by two people while the ship was stationery during a CTD cast, with one person holding the Zoom F3 sound recorder and another person holding a monopod with the microphone's cable wrapped around it, slowly lowering down until the microphone bobbed about 1-3 meters below the surface of the ocean. Deck drop recordings lasted 7-22 minutes. These recordings included strong ambient boat noise from the thrusters; the software Audacity was used to edit the files and highlight frequencies of interest. Underwater photography was used during one CTD cast, with a GoPro cube attached to the bottom of the CTD rosette in water-tight housing, along with two water-tight housings for lights and their batteries. Madeline will continue to work with this aural and visual artistic dataset to create multimedia work, sharing both online and in gallery and performance spaces to continue long-term outreach activities beyond the cruise.

Bhavna played a pivotal role in launching and maintaining digital outreach. She collaborated with the NSF communications specialist and Polar STEAM personal to establish an Instagram account, utilizing NSF-approved tags such as #NSF, #NSFfunded, #PolarSTEAM, #USAP, and #NABP2411.

Instagram. The page, VisitPalmer24, featured over 100 posts, reels, and stories. These posts included pictures, videos, and narratives about science labs, experiments, and daily life aboard the research vessel. The account reached 243 followers and 417 accounts followed, with an average of 200 viewers per story and peaks of up to 1.5K viewers for specific stories. Daily clicks on the account averaged 1,000.

Blogs. Bhavna authored two blog posts to highlight the expedition's collaborative efforts and scientific significance:

The Power of Collaboration in Antarctic Research (https://visitpalmer24.wordpress.com/): This post reached 150 views in its first week.

Journey to the Southern Ocean: Exploring the Microscopic Life of Phytoplankton (https://polarsteam.info/journey-to-the-southern-ocean-exploring-the-microscopic-life-of-phytoplankton/): Garnered **187 views** within 10 days of publication.

Flickr. Bhavna also opened a Flickr account with PolarSTEAM, posted photos and videos to document the expedition. Uploads: Over 200 photos and videos documenting the research and daily life onboard. Weekly Stats: Achieved 300+ views in its first week

Community and Educational Outreach. Bhavna developed and delivered a PowerPoint presentation titled *Science on a Ship* for local high schools to share insights about life aboard a research vessel and the importance of phytoplankton in Antarctic ecosystems. She also designed hands-on learning materials for middle school students, such as the "Types of Phytoplankton: From Google Search to Plantoscope" to make the topic accessible and engaging.

Educational Development and Interdisciplinary Projects. Upon returning to shore, Bhavna will develop educational resources and labs for her chemistry classes at Lone Star Community College. She has been working on developing chemical labs such as *Investigating Iron as a Limiting Nutrient for Phytoplankton in the Southern Ocean* for introductory and general chemistry courses. She introduced the chlorophyll *a* molecule in her organic chemistry classes, including its hydrolysis and photosynthesis reactions.

Bhavna is spearheading an interdisciplinary project involving faculty and students from multiple departments. For the chemistry department, they will analyze the effect of nutrients like iron, nitrate, and phosphate on phytoplankton growth in the Gulf of Mexico and compare their responses to phytoplankton from the Southern Ocean. For the biology department, they will study phytoplankton colonies and their growth in specific environmental conditions, particularly in the Australian Antarctic Region (AAR). For the environmental Science department, they will conduct trace metal data analysis related to hydrothermal vents. For the computer Science department, they will create simulations of ocean currents, temperature, and hydrothermal vents in the AAR region. For the mathematics department, they will use MATLAB to plot and analyze profiles of temperature, salinity, density, fluorescence, dissolved oxygen, and turbidity, examining their impact on the AAR ecosystem.

Students will present their interdisciplinary projects at an *Octoberfest* event, inviting local community members, students, and the local public. Over 1000 people attend this *Octoberfest* every year. These presentations aim to inform and engage audiences on the importance of Antarctic research and inspire young scientists.

Outcomes and Future Plans. The outreach activities effectively reach diverse audiences through digital platforms, educational materials, and interdisciplinary collaboration. With over 1,000 daily Instagram clicks, hundreds of blog and Flickr views, and strong student engagement in educational activities, the outreach activities exceeded expectations.

References

Alderkamp, A-C, GL van Dijken, KE Lowry, TL Connelly, M Lagerström, RM Sherrell, T Haskins, E Rogalsky, O Schofield, S Stammerjohn, PL Yager, KR Arrigo (2015) Fe availability drives phytoplankton photosynthesis rates during spring bloom in the Amundsen Sea Polynya, Antarctica. *Elementa: Science of the Anthropocene,* doi:10.12952/journal.elementa.000043

Altmann, H.J. (1972) Bestimmung von in Wasser gel¨ostem Sauerstoff mit Leukoberbelinblau I. *Fresenius Z. Für Anal. Chem*. 262, 97–99. https://doi.org/ 10.1007/BF00425919.

Andrews-Goff, V, S Bestley, NJ Gales, SM Laverick, D Paton, AM Polanowski, NT Schmitt, MC Double (2018) Humpback whale migrations to Antarctic summer foraging grounds through the southwest Pacific Ocean, *Scientific Reports* 8, 12333.

Ardyna, M, L Lacour, S Sergi, F d'Ovidio, J-B Sallée, M Rembauville, S Blain, A Tagliabue, R Schlitzer, C Jeandel, KR Arrigo, H Claustre (2019) Hydrothermal vents trigger massive phytoplankton blooms in the Southern Ocean. *Nat. Comm.* 10, 2451, doi:10.1038/s41467-019-09973-6.

Arrigo, KR, DH Robinson, DL Worthen, RB Dunbar, GR DiTullio, M VanWoert, MP Lizotte (1999) Phytoplankton community structure and the drawdown of nutrients and CO_2 in the Southern Ocean. *Science* 283, 365-367.

Arrigo, KR, DL Worthen, DH Robinson (2003) A coupled ocean-ecosystem model of the Ross Sea: 2. Iron regulation of phytoplankton taxonomic variability and primary production. *J. Geophys. Res.* 108 C10, 3316, 10.1029/2001JC001138

Arrigo, KR, GL van Dijken, S Bushinsky (2008a) Primary Production in the Southern Ocean, 1997-2006. *J. Geophys. Res*. 113. C08004, doi:10.1029/2007JC004551.

Bennett, SA, EP Achterberg, DP Connelly, PJ Statham, GR Fones, CR German (2008) The distribution and stabilisation of dissolved Fe in deep-sea hydrothermal plumes, *Earth Planet. Sci. Lett.* 270, 157–167.

Blain, S, P Tréguer, S Belviso, E Bucciarelli, M Denis, S Desabre, M Fiala, V Martin Jézéquel, J Le Fèvre, P Mayzaud, J-C Marty, S Razouls (2001) A biogeochemical study of the island mass effect in the context of the iron hypothesis: Kerguelen Islands, Southern Ocean. *Deep-Sea Res. Part I*, 48, 163-187

Blain, S, B Quéguiner, L Armand, S Belviso, B Bombled, L Bopp, A Bowie, C Brunet, C Brussaard, F Carlotti, U Christaki, A Corbière, I Durand, F Ebersbach, J-L Fuda, N Garcia, L Gerringa, B Griffiths, C Guigue, C Guillerm, S Jacquet, C Jeandel, P Laan, D Lefèvre, C Lo Monaco, A Malits, J Mosseri, I Obernosterer, Y-H Park, M Picheral, P Pondaven, T Remenyi, V Sandroni, G Sarthou, N Savoye, L Scouarnec, M Souhaut, D Thuiller, K Timmermans, T Trull, J Uitz, P van Beek, M Veldhuis, D Vincent, E Viollier, L Vong, T Wagener (2007) Effect of natural iron fertilization on carbon sequestration in the Southern Ocean. *Nature* 446, 1070–1074.

Boyd, PW, T Jickells, CS Law, S Blain, EA Boyle, KO Buesseler, KH Coale, JJ Cullen, HJW de Baar, M Follows (2007) Mesoscale iron enrichment experiments 1993-2005: Synthesis and future directions. *Science* 315(5812), 612-617.

Boyd, PW, KR Arrigo, R Strzepek, GL van Dijken (2012) Mapping phytoplankton iron utilization: Insights into Southern Ocean supply mechanisms, *J. Geophys. Res*. 117, C06009, doi:10.1029/2011JC007726.

Boyle, EA, BA Bergquist, RA Kayser, N Mahowald (2005) Iron, manganese, and lead at Hawaii Ocean time-series station ALOHA: Temporal variability and an intermediate water hydrothermal plume. *Geochim. Cosmochim. Acta* 69, 933_952.

Boyle, EA, WK Jenkins (2008) Hydrothermal iron in the deep western South Pacific. *Geochim. Cosmochim. Acta* 72, A107.

Browning, T.J., Achterberg, E.P., Engel, A., Mawji, E. (2021) Manganese co-limitation of phytoplankton growth and major nutrient drawdown in the Southern Ocean. *Nature Communications.* 12(1), 884. https://doi.org/10.1038/s41467-021-21122-6.

Buck NJ, PM Barrett, PL Morton, WM Landing, JA Resing (2021) Energy dispersive X-ray fluorescence methodology and analysis of suspended particulate matter in seawater for trace element compositions and an intercomparison with high-resolution inductively coupled plasma-mass spectrometry. *Limnol. Oceanogr. Methods*, 19 (6), 401-415.

de Baar, HJW, JTM de Jong, DCE Bakker, BM Löscher, C Veth, U Bathmann, V Smetacek (1995) Importance of iron for plankton blooms and carbon dioxide drawdown in the Southern Ocean. *Nature* 373, 412–415.

Duce, RA, NW Tindale (1991) Atmospheric transport of iron and its deposition in the ocean. *Limnol. Oceanogr.* 36, 1715–1726.

Elderfield, H, A Schultz (1996) Mid-ocean ridge hydrothermal fluxes and the chemical composition of the ocean. *Annu. Rev. Earth Planet. Sci*. 24, 191-224.

Frölicher, TL, JL Sarmiento, DJ Paynter, JP Dunne, JP Krasting, M Winton (2014) Dominance of the Southern Ocean in Anthropogenic Carbon and Heat Uptake in CMIP5 Models. *J. Clim.* 28, 862-886.

Gaiero, DM, JL Probst, PJ Depetris, SM Bidart, L Leleyter (2003) Iron and other transition metals in Patagonian riverborne and windborne materials: geochemical control and transport to the southern South Atlantic Ocean. *Geochim. Cosmochim. Acta* 67, 3603–3623.

Holm-Hansen, O., Lorenzen, C. J., Holmes, R. W., & Strickland, J. D. H. (1965) Fluorometric determination of chlorophyll. *ICES Journal of Marine Science*, 30(1), 3–15. https://doi.org/10.1093/icesjms/30.1.3

Irisson, J.-O., L. Salinas, S. Colin, Team Complex, M. Picheral (2022) EcoTaxa: a tool to support the taxonomic classification of large datasets through supervised machine learning. *SF Ecologie* 2022, Metz, France. ⟨hal-04026447⟩.

Jones, M.R., Luther, G.W., Mucci, A., Tebo, B.M. (2019) Concentrations of reactive Mn(III)-L and MnO_2 in estuarine and marine waters determined using spectrophotometry and the leuco base, leucoberbelin blue. *Talanta,* 200, 91-99. https://doi.org/10.1016/j.talanta.2019.03.026.

Klunder MB, P Laan, R Middag, HJW De Baar, JC van Ooijen (2011) Dissolved iron in the Southern Ocean (Atlantic sector). *Deep-Sea Res. Part II* 58, 2678–2694.

Landschützer, P, N Gruber, FA Haumann, C Rödenbeck, DCE Bakker, S van Heuven, M Hoppema, N Metzl, C Sweeney, T Takahashi, B Tilbrook, R Wanninkhof (2015) The reinvigoration of the Southern Ocean carbon sink. *Science* 349, 1221-1224.

Lannuzel, D, V Schoemann, J de Jong, L Chou, B Delille (2008) Iron study during a time series in the western Weddell pack ice. *Mar. Chem.* 108, 85–95.

Lannuzel, D, M Vancoppenolle, P van der Merwe, J de Jong, KM Meiners, M Grotti, J Nishioka, V Schoemann (2016) Iron in sea ice: Review and new insights. *Elementa Science of the Anthropocene*. 4, 000130, doi: 10.12952/journal.elementa.000130elementascience.org.

Martin, JH, RM Gordon, SE Fitzwater (1990) Iron in Antarctic waters. *Nature* 345, 156-158.

Measures, CI, Yuan, JC, Resing, JA. (1995) Determination of Iron by Flow Injection Analysis, Marine Chemistry, 50, 3-12.

Moore, JK, MR Abbott (2000) Phytoplankton chlorophyll distributions and primary production in the Southern Ocean. *J. Geophys. Res.* 105, 28709-28722

Oldham, V.E., Chmiel, R., Hansel, C.M., DiTullio, G.R., Rao, D., Saito, M. (2021) Inhibited manganese oxide formation hinders cobalt scavenging in the Ross Sea. *Global Biogeochemical Cycles.* 35(5). e2020GB006706. https://doi.org/10.1029/2020GB006706.

Orsi, AH, T Whitworth III, WD Nowlin Jr. (1995) On themeridional extent and fronts of the Antarctic Circumpolar Current. *Deep-Sea Res. Part I* 42 (5), 641–673.

Pavia, FJ, RF Anderson, EE Black, LE Kipp, SM Vivancos, MQ Fleisher, MA Charette, V Sanial, WS Moore, M Hult, Y Lu, H Cheng, P Zhang, RL Edwards (2019) Timescales of hydrothermal scavenging in the South Pacific Ocean from [234]Th, [230]Th, and [228]Th. *Earth Planet Sci Lett*, 506, 146–156.

Pollina, T, AG Larson, F Lombard, H Li, D Le Guen, S Colin, C de Vargas, M Prakash (2022) PlanktoScope: Affordable Modular Quantitative Imaging Platform for Citizen Oceanography. *Front. Mar. Sci*., 9, https://doi.org/10.3389/fmars.2022.949428

Schine, CMS, A-C Alderkamp, G van Dijken, LJA Gerringa, P Laan, H van Haren, WH van de Poll, KR Arrigo (2021) Massive Southern Ocean phytoplankton bloom fed by iron of possible hydrothermal origin. *Nature Comm.*, https://doi.org/10.1038/s41467-021-21339-5.

Smith, J, BH Robison, JJ Helly, RS Kaufmann, HA Ruhl, TJ Shaw, BS Twining, M Vernet (2007) Free-drifting icebergs: hot spots of chemical and biological enrichment in the Weddell Sea. *Science* 317, 478–482.

Smith, WO, Jr., LI Gordon (1997) Hyperproductivity of the Ross Sea (Antarctica) Polynya during austral spring, *Geophys. Res. Lett*. *24*, 233–236.

Sokolov, S, SR Rintoul (2007) On the relationship between fronts of the Antarctic Circumpolar Current and surface chlorophyll concentrations in the Southern Ocean. *J. Geophys. Res.* 112, C07030.

Statham, PJ, CR German, DP Connelly (2005) Iron(II) distribution and oxidation kinetics in hydrothermal plumes at the Kairei and Edmond vent sites, Indian Ocean. *Earth Planet. Sci. Lett*. 236, 588_596.

Stookey, L.L. (1970) Ferrozine---a new spectrophotometric reagent for iron. *Analytical Chemistry.* 42(7), 779-781. https://doi.org/10.1021/ac60289a016.

Sweeney, C (2003) The annual cycle of surface water CO_2 and O_2 in the Ross Sea: A model for gas exchange on the continental shelves of Antarctica. In: Biogeochemistry of the Ross Sea (Dunbar R.B. and Ditullio R.G., eds) *Ant. Res. Ser.* 78, 295-312

Tagliabue, A, J Resing (2016) Impact of hydrothermalism on the ocean iron cycle. *Phil. Trans. Royal Soc. A: Mathematical, Physical and Engineering Sciences*, 374(2081). https://doi.org/10.1098/rsta.2015.0291

Tagliabue, A, L Bopp, J-C Dutay, AR Bowie, F Chever, P Jean-Baptiste, E Bucciarelli, D Lannuzel, T Remenyi, G Sarthou, O Aumont, M Gehlen, C Jeandel (2010) Hydrothermal contribution to the oceanic dissolved iron inventory. *Nature Geosci*. 3, 252–256.

Tagliabue, A, O Aumont, R DeAth, JP Dunne, S Dutkiewicz, E Galbraith, K Misumi, JK Moore, A Ridgwell, E Sherman, C Stock, M Vichi, C Völker, A Yool (2016) How well do global ocean biogeochemistry models simulate dissolved iron distributions? *Global Biogeochem. Cycles* 30, 149–174, https://doi.org/10.1002/2015GB005289.

Takahashi, T. et al. Climatological mean and decadal change in surface ocean pCO2, and net sea–air CO2 flux over the global oceans (2009). *Deep-Sea Res. Part II*, 56, 554-577.

Thibault de Chanvalon, A., & Luther, G. W. (2019). Mn speciation at nanomolar concentrations with a porphyrin competitive ligand and UV–vis measurements. *Talanta*, 200, 15–21. https://doi.org/10.1016/j.talanta.2019.02.069.

Toner, BM, SC Fakra, SJ Manganini, CM Santelli, MA Marcus, JW Moffett, O Rouxel, CR German, KJ Edwards (2009) Preservation of iron(II) by carbon- rich matrices in a hydrothermal plume. *Nat. Geosci*. 2(3), 197–201.

Tynan, CT (1998) Ecological importance of the Southern Boundary of the Antarctic Circumpolar Current. *Nature* 392(6677), 708-710.